Regulation and mechanistic basis of macrolide resistance by the ABC-F ATPase MsrD

Corentin R. Fostier[1], Farès Ousalem[1], Elodie C. Leroy[2], Saravuth Ngo[1], Heddy Soufari[2,3], C. Axel Innis[2], Yaser Hashem[2,*], Grégory Boël[1,4,*]

[1]UMR 8261, CNRS, Université de Paris, Institut de Biologie Physico-Chimique, 75005 Paris, France

[2]INSERM U1212 (ARNA), Institut Européen de Chimie et Biologie, Université de Bordeaux, 33607 Pessac, France

[3]Current address: NovAliX, Boulevard Sébastien Brant, Bioparc, 67405 Illkirch Cedex, France

[4]Lead contact

*Correspondence:

Grégory Boël, Institut de Biologie Physico-Chimique, 13 rue Pierre et Marie Curie, 75005 Paris, France, tel. : +33 (0) 1 58 41 51 21; e-mail: boel@ibpc.fr

Yaser Hashem, Institut Européen de Chimie et Biologie, Université de Bordeaux, 33607 Pessac, France, tel. : +33 (0) 5 40 00 88 22; e-mail: yaser.hashem@inserm.fr

SUMMARY

Antibiotic resistance ABC-Fs (ARE ABC-Fs) are translation factors currently proliferating among human pathogens that provide resistance against clinically important ribosome-targeting antibiotics. Here, we combine genetic and structural approaches to determine the activity of the *streptococcal* ARE ABC-F protein MsrD on the ribosome and its regulation in response to macrolide exposure. We show that cladinose-containing macrolides lead to insertion of MsrDL leader peptide into a conserved crevice of the ribosomal exit tunnel, which remained thus far undocumented, concomitantly with 23S rRNA rearrangements that preclude proper accommodation of release factors and inhibits termination. The stalled ribosome obstructs formation of a Rho-independent terminator which prevents *msrD* transcriptional attenuation. This stalled ribosome is rescued by MsrD powered by its two functionally asymmetric ATPase sites, but not by MsrD mutants which do not provide antibiotic resistance, showing evidence of equivalence between MsrD function in antibiotic resistance and its action on this complex.

KEYWORDS

Ribosome, protein synthesis, antibiotic resistance, ARE ABC-F protein family, leader peptide, cryo-EM.

41 **INTRODUCTION**

42 ABC-F ATPases belonging to the ATP-Binding Cassette (ABC) superfamily are
43 translation factors and some of them, termed antibiotic resistance ABC-Fs (ARE ABC-Fs),
44 confer resistance to clinically important antibiotics that bind to the ribosomal peptidyl
45 transferase center (PTC) and/or the nascent peptide exit tunnel (NPET) (Crowe-McAuliffe et
46 al., 2018, 2021; Sharkey et al., 2016; Su et al., 2018). ABC-F proteins are composed of two
47 ABC domains (or Nucleotide Binding Domains, NBDs) joined by a linker region called P-site
48 tRNA-interaction motif (PtIM) (Boël et al., 2014; Chen et al., 2014), also named antibiotic
49 resistance determinant (ARD) for ARE ABC-Fs (Crowe-McAuliffe et al., 2018, 2021). The two
50 ABC domains dimerize after binding of two ATP molecules and in this conformation the factor
51 can bind the ribosomal E-site (Chen et al., 2014), where the PtIM adopts an α-helical hairpin
52 conformation that interacts directly with the peptidyl-tRNA and extends toward the PTC/NPET.
53 Three antibiotic resistance phenotypes are associated with ARE ABC-Fs: (i) MKS_B
54 (Macrolides, Ketolides, Streptogramins group B); (ii) PLS_A (Pleuromutilins, Lincosamides,
55 Streptogramins group A); (iii) PhO (Phenicols, Oxazolidinones) (Fostier et al., 2021; Ousalem
56 et al., 2019). However, despite structural investigations (Crowe-McAuliffe et al., 2018, 2021;
57 Su et al., 2018), the exact molecular mechanism of action of ARE ABC-Fs remains unclear,
58 so is their genetic regulation.

59 Over the last forty years, biochemical and structural investigations demonstrated the
60 ability of elongating nascent chains (NC) into the ribosomal tunnel to interact with metabolites
61 or antibiotics, thus adapting protein synthesis to environmental cues (Arenz et al., 2014a, 2016;
62 Beckert et al., 2021; Herrero del Valle et al., 2020; van der Stel et al., 2021). In human
63 pathogens, antibiotic-dependent formation of stalled ribosome complexes (SRCs) on
64 regulatory ORFs, named leader peptides, can subsequently allow regulation of downstream
65 resistance genes in response to antibiotic exposure (Horinouchi and Weisblum, 1980; Ito and
66 Chiba, 2013; Narayanan and Dubnau, 1985; Vazquez-Laslop et al., 2008).

67 ARE ABC-F gene *msrD* is a member of the *msr* (macrolide and streptogramin B
68 resistant) gene group previously referred as *mel* (Gay and Stephens, 2001; Roberts et al.,

69 1999). This gene is generally found in operon with a macrolide efflux facilitator (*mefA* or *mefE)*
70 *gene*, the two corresponding proteins acting synergistically to confer macrolide resistance
71 (Daly et al., 2004; Nunez-Samudio and Chesneau, 2013; Tatsuno et al., 2018; Zhang et al.,
72 2016). This operon is part of the Macrolide Efflux Genetic Assembly (MEGA) (Del Grosso et
73 al., 2004, 2006) that disseminates in human pathogens on mobile genetic elements:
74 conjugative transposons like the tn916-type (Chancey et al., 2015a) and conjugative
75 prophages like the Φ1207.3 (Iannelli et al., 2014) among streptococci, conjugative plasmids
76 like the pMUR050 (González-Zorn et al., 2005) among enterobacteria. In streptococci, the
77 operon is transcribed in presence of erythromycin (ERY) as a polycistronic mRNA from a single
78 promoter located ~350 bp upstream *mefA* (Ambrose et al., 2005; Chancey et al., 2015b). It is
79 also regulated by ribosome-mediated transcription attenuation via MefAL leader peptide
80 (MTASMRLR), which is closely related to ErmDL leader peptide (MTHSMRLRFPTLNQ), both
81 peptides harboring the characteristic macrolide-arrest motif "RLR" (Beckert et al., 2021;
82 Chancey et al., 2015b; Ramu et al., 2009; Sothiselvam et al., 2014).

83 Here, we report the presence of a second transcriptional attenuator on the *mefA/msrD*
84 operon regulating exclusively *msrD* expression upon macrolide exposure. Presence of ERY
85 induces ribosome stalling on the previously identified *msrDL* leader peptide (encoding
86 MYLIFM) (Ramu et al., 2009), allowing RNA polymerase (RNAP) to bypass an intrinsic
87 terminator. Our findings demonstrate stalling occurs due to hampered translation termination
88 on UAA stop codon, action of both release factors 1 and 2 (RF1 and RF2) being inhibited. Our
89 results are supported by the cryo-EM structure of MsrDL-SRC that provides molecular insight
90 on how the PTC precludes productive accommodation of RF1/RF2 and how the NC
91 discriminates tunnel-bound cladinose-containing macrolides. The path of the NC within the
92 tunnel greatly differs from previously described leader peptides (Arenz et al., 2014a, 2016;
93 Beckert et al., 2021; Herrero del Valle et al., 2020; van der Stel et al., 2021) with the NC
94 latching into a ribosomal crevice, conserved from prokaryotes to eukaryotes, delimited by 23S
95 rRNA nucleotides U2584, U2586, G2608 and C2610 that may form a novel ribosomal
96 functional site. Finally, our results demonstrate that the two ATPase sites of MsrD perform

97 different functions and the protein can negatively self-regulate its synthesis in presence of ERY
98 by direct action on MsrDL-stalled ribosomes.
99
100 **RESULTS**
101 **MsrD provides macrolide and ketolide resistance by direct interaction with ribosome**
102 The *mefA/msrD* macrolide resistance operon (**Figure 1A**) is part of the MEGA element
103 currently spreading among clinical isolates and livestock (de Block et al., 2021; Chancey et al.,
104 2015b; Lu et al., 2010; Sharma et al., 2020). A phylogenetical analysis (**Figure S1A**) shows
105 that the operon disseminates predominantly in Gram-positive firmicutes (mostly streptococci)
106 and in some Gram-negative proteobacteria (such as *Haemophilus influenzae, Neisseria*
107 *gonorrhoeae or Escherichia coli*). Gene *msrD* shares ~62 % identity with its closest homolog
108 *msrE* (Su et al., 2018), both factors exhibiting the canonical ABC-F organization (**Figure 1B**).
109 Model bacteria *E. coli* presents undeniable advantages for genetic and molecular
110 biology, but presence of multidrug efflux systems greatly limits its use in antibiotic research
111 (Nikaido, 2009; Nikaido and Pagès, 2012). To circumvent this limitation, we took advantage of
112 *E. coli* DB10 strain which exhibits exacerbated sensitivity to macrolide antibiotics (Datta et al.,
113 1974). Heterologous expression of *msrD* from an arabinose-inducible promoter conferred
114 macrolide and ketolide resistance phenotype to *E. coli* DB10 strain (**Table 1**), demonstrating
115 the functionality of the factor in this organism. Expression of *msrD* resulted in 8-fold minimal
116 inhibitory concentration (MIC) increase for 14-membered macrolide ERY, 8-fold for 15-
117 membered macrolide azithromycin (AZI) and 2-fold for telithromycin (TEL, ketolide antibiotic
118 derived from 14-membered macrolides). However, no change in MIC was observed for 16-
119 membered macrolides tylosin (TYL) and spiramycin (SPI), neither for non-macrolide antibiotics
120 lincomycin (LNC), linezolid (LNZ) and retapamulin (RTP) (**Table 1**).
121 Polysome profile from bacteria exposed to ERY show a stabilization of ribosome
122 disomes (**Figure 1C**) as expected for an antibiotic that inhibits ribosome elongation. The
123 disomes accumulation likely results from elongating ribosomes that collide on ERY-stalled
124 ribosomes. Induction of *msrD* alleviates the accumulation of disomes and restores a profile

125 identical to that without ERY (**Figure 1D**). Western blots of the polysome fractions show an
126 MsrD association with the 70S ribosome and the 50S subunit with a higher affinity for the latter
127 one. These results agree with a model in which MsrD directly rescues ERY-stalled ribosomes
128 and that MsrD can restore normal translation in presence of the antibiotic.

129 To understand the function of the ATPase activity of MsrD, we constructed ATPase-
130 deficient variants $MsrD_{E125Q}$, $MsrD_{E434Q}$ and $MsrD_{E125Q/E434Q}$ (hereafter referred as $MsrD_{EQ2}$) by
131 replacing the catalytic glutamic acid residue (E) in Walker B motif of each or both ABC domain
132 by a glutamine (Q) (**Figures 1B** and **S1B**). This mutation strongly reduces the ATP hydrolysis
133 while preserving the local stereochemistry of active site and has been extensively used to trap
134 ABC-F factors on the ribosome in ATP-bound conformation (Chen et al., 2014; Crowe-
135 McAuliffe et al., 2018, 2021). Expression of $msrD_{EQ2}$ in absence of ERY shows an
136 accumulation of disomes and western-blotting reveals its association with the 30S subunit,
137 70S ribosome and polyribosomes. This result shows that $MsrD_{EQ2}$ binds to the ribosome and
138 inhibits its elongation (**Figure 1E**) as observed for all reported ABC-F carrying the E-to-Q
139 mutation (Boël et al., 2014; Murina et al., 2019), with the exception of MsrE (Su et al., 2018).
140 Expression of $msrD_{EQ2}$ also alters the 30S peak, an alteration often observed during translation
141 inhibition and presumably due to pre-30S maturation defects (Siibak et al., 2009). In presence
142 of ERY, the disome and trisome accumulation increases and western blots show an increase
143 of $MsrD_{EQ2}$ in the disome fraction (**Figure 1E**, fraction 13). Still, the ATPase activity of MsrD
144 impacts its binding affinity, MsrD having a higher affinity for the 50S subunit in contrast to
145 $MsrD_{EQ2}$ having a higher affinity for the 70S ribosome (**Figures 1D** and **E**). A model consistent
146 with these observations would imply that MsrD binds to ERY-stalled ribosomes in an ATP-
147 bound close conformation without the need of its ATPase activity, then ATPase activity triggers
148 70S dissociation, MsrD staying associated with the 50S subunit. Similar results were observed
149 by expressing *msrD* and $msrD_{EQ2}$ in *E. coli* K12 MG1655 (**Figure S1C**) without the presence
150 of ERY. They also show a decrease of the 70S peak correlated with an increase of 30S and
151 50S peaks for *msrD* condition when compared to the control, supporting the proposed
152 dissociation model. Western blots show more $MsrD_{EQ2}$ than MsrD in total lysates (**Figures 1D**

153 and **E**), $MsrD_{EQ2}$ inhibiting protein synthesis and therefore its own synthesis, we hypothesized
154 that $MsrD_{EQ2}$ is less expressed but more soluble, which has been confirmed with a solubility
155 test (**Figure S1D**).

156 We evaluated the influence of E-to-Q mutations of MsrD on bacterial growth and the
157 antibiotic resistance phenotype. All the mutations impair bacterial growth and antibiotic
158 resistance phenotype (**Figure 1F**), while $MsrD_{E125Q}$ and $MsrD_{EQ2}$ have a similar effect on
159 bacterial growth in absence or at low ERY concentration, $MsrD_{E434Q}$ is more toxic. However,
160 $MsrD_{E125Q}$ variant maintains some resistance (MIC = 4 μM) compared to control (MIC = 2 μM)
161 which is also supported by the fact that $MsrD_{E125Q}$ IC_{50} is ~8 times higher than Control IC_{50}
162 (**Figure 1F**, **Supplemental Table 1**). The two ATP hydrolysis sites (**Figure S1B**) have
163 therefore different tasks and are functionally asymmetric, ATP site II achieving in part the
164 mechanism of ERY-stalled ribosome rescue. We also evaluated the importance of other
165 residues of MsrD. Truncation of the PtIM (replaced by three glycine) or just the Loop (ΔPtIM,
166 ΔLoop respectively) completely abolished the resistance phenotype *in vivo* as reported *in vitro*
167 for MsrE (Su et al., 2018) (**Figure 1G**). Punctual mutations in the Loop (**Figure 1B**) affect the
168 resistance to a different extent, mutation of R241 into alanine has almost no effect on the
169 phenotype, but equivalent mutation for L242 or H244 reduces IC_{50} by ~3 fold (**Figure 1H** and
170 **Supplemental Table 1**), demonstrating that these residues are important for MsrD function,
171 but not essential even if they are predicted at the vicinity of the antibiotic (**Figure S1E**) in the
172 MsrE-ribosome complex (Su et al., 2018). Interestingly, this finding contrasts with mutagenesis
173 assays for MsrE showing that mutation R241A reduces the resistance by more than 50%.
174 Replacement of H244 by the larger residue tryptophan should displace the drug by steric
175 occlusion, but the variant lost most of its antibiotic resistance phenotype (**Figure 1H**). Similarly,
176 MsrD does not provide resistance to TYL nor SPI (**Table 1**), while both antibiotics should clash
177 with MsrD according to MsrE structure (**Figure S1E**). Same observation can be made with
178 LNC, LNZ or RTP (**Table 1** and **Figure S1E**). Therefore, MsrD action on the antibiotic is indirect
179 and direct steric occlusion to displace the antibiotic seems excluded.

180 **Ribosome-mediated transcriptional attenuation regulates *msrD* expression**

181 Analysis of the *mefA/msrD* operon sequence exposes a stringent ribosome binding site
182 (RBS, whose sequence is 5'-GGAGGA-3') only 8 bp downstream *mefA* stop codon and
183 possibly required for translation of the downstream putative small ORF *msrDL* (**Figure S2A**).
184 In order to test the influence of *msrDL* on *msrD* expression, a fluorescent reporter, which
185 contains the sequence spanning from the first nucleotide downstream *mefA* stop codon to
186 *msrD* three first codons fused to the Yellow Fluorescent Protein gene (YFP), was cloned in the
187 low copy pMMB plasmid (Fürste et al., 1986) under the control of an IPTG-inducible promoter
188 (**Figure 2A**). The resulting plasmid, pMMB-*msrDL-msrD*$_{(1-3)}$:*yfp,* was used to directly follow the
189 fluorescence reflecting *yfp* expression.

190 Basal fluorescence level was found stable in *E. coli* DB10 strain containing pMMB-
191 *Control* independently of ERY concentration (**Figure 2A**) while a fluorescence increase
192 correlated with ERY concentration was observed in cells containing pMMB-*msrDL-msrD*$_{(1-}$
193 $_{3)}$:*yfp*, indicating an ERY-dependent induction (**Figure 2A**). Optimal induction was found at 100
194 nM ERY while only 6.25 nM was sufficient to significantly induce *msrD*$_{(1-3)}$:*yfp* expression,
195 demonstrating the high sensitivity of the system toward its inducer. Moreover, a reduced but
196 significative fluorescence signal was detected at 0 nM ERY indicating an imperfect repression.
197 These results are consistent with previous description of *ermC* induction by nanomolar ERY
198 concentrations in *S. aureus* and *B. subtilis* (Mayford and Weisblum, 1989; Weisblum et al.,
199 1971), contrary to *E. coli* strains JM109 and RR1 where micromolar concentrations are
200 required (Bailey et al., 2008; Kirsch and Lai, 1984). Inactivation of *msrDL* ORF by replacement
201 of the start codon by an amber stop codon (pMMB-*msrDL*$_{(no_ORF)}$-*msrD*$_{(1-3)}$:*yfp*) resulted in the
202 elimination of the fluorescence induction (**Figure 2A**), demonstrating that *msrDL* translation is
203 an important and necessary cis-acting feature to regulate *msrD*$_{(1-3)}$:*yfp* expression as reported
204 for *ermC* (Dubnau, 1985).

205 In bacteria, antibiotic-dependent gene induction relies mainly on translational or
206 transcriptional attenuation (Dersch et al., 2017). To determine if MsrDL prompts a
207 transcriptional or translational attenuation, northern blots analysis with a probe located in

208 *msrD*$_{(1-3)}$:*yfp* 3' UTR were performed on total RNA extracted from cell exposed or not to ERY
209 and/or IPTG. A 1.2-kb band corresponding to *msrDL-msrD*$_{(1-3)}$:*yfp* mRNA is transcribed in
210 presence of IPTG and starts to increase steadily 5 min after exposure to 100 nM ERY (**Figure**
211 **2B**). Consistent with this ERY-dependent transcript accumulation, we concluded that *msrD*
212 regulation by *msrDL* occurs at the transcription level.

213 Transcription attenuation employs premature transcription termination via: (i) Rho-
214 dependent terminator (RDT) by binding of Rho factor, a RecA-type ATPase, to a C-rich and
215 G-poor sequence known as Rho utilization site (Banerjee et al., 2006); (ii) Rho-independent
216 terminator (RIT) where a stable GC-rich stem-loop followed by a poly-uridine sequence causes
217 RNAP to drop off (Ray-Soni et al., 2016). Treatment with bicyclomycin, a Rho inhibitor, did not
218 result in constitutive expression of the reporter, thus excluding the possibility of RDT
219 attenuation (**Figure S2B**). Analysis of the intergenic region between *msrDL* and *msrD* using
220 ARNold server (Naville et al., 2011) revealed the presence of a RIT with a ΔG of -7.9 kcal.mol^{-}
221 ^{1} (**Figure 2C**). In order to test this possible transcription termination activity, we generated a
222 mutant by removing the putative terminator (referred as pMMB-msrDL$_{(no_term)}$-msrD$_{(1-3)}$:*yfp*).
223 Deletion of the terminator resulted in a constitutive expression of the fluorescent reporter in
224 absence of ERY, indicating that the terminator is a necessary cis-acting regulatory feature that
225 can terminate transcription (**Figure 2C**). These results validate the presence of a second
226 transcriptional attenuator in the *mefA*/*msrD* operon that regulates only *msrD*.

227

228 **Selective drug-sensing by MsrDL prevents its translation termination**

229 To determine how this regulation occurs via ribosome-mediated mechanism,
230 translation of *msrDL* mRNA with the PURE system (Shimizu et al., 2001) was subjected to
231 various antibiotics and its propensity to form SRC was analyzed by toeprinting (Hartz et al.,
232 1988) (**Figure 3** and **Figure S3**). A strong toeprint signal was observed in presence of ERY
233 and AZI, while it was absent in presence of TEL, TYL and SPI (**Figure 3A**). This *in vitro* result
234 is correlated to *in vivo* observations made with the *msrD*$_{(1-3)}$:*yfp* reporter gene which was also

235 only induced by ERY and AZI, but not by TEL, TYL, SPI and non-macrolide antibiotics (**Figure**
236 **3B**).

237 We further characterized the translation of *msrDL* mRNA and showed that in presence
238 of 50 µM RTP, an inhibitor of the first peptide bond formation which allows to identify ORFs
239 start codon (Meydan et al., 2019), a clear toeprint occurred (**Figure 3C**). This toeprint
240 corresponds to a ribosome stalled with the initiating codon in the ribosomal P site and confirms
241 that ribosomes can initiate *msrDL* translation. The toeprint observed at positions +31, +32 and
242 +33 relative to *msrDL* 5' end (**Figures 3A** and **C**) in presence of ERY and AZI indicates an
243 SRC located at the termination step of MsrDL synthesis with the C-terminal methionine (M6)
244 codon in the P site and UAA stop codon in the A site. In accordance with this, reactions
245 depleted of release factors (RF1, RF2, RF3) (**Figure 3C**) show the same toeprint result.
246 Moreover, addition of puromycin led to the loss of this toeprint signal, while preserving it in
247 presence of ERY (**Figure 3C**). Puromycin is an aminonucleoside antibiotic mimicking A site
248 substrate tyrosyl-tRNA and causing premature chain termination. While actively translating
249 ribosomes are sensitive to this antibiotic, stalled ones tend to be refractory (Muto et al., 2006;
250 Seip and Innis, 2016; Vazquez-Laslop et al., 2008). The resistance of MsrDL-SRC to
251 puromycin is consistent with an ERY-sensing NC that leads to PTC silencing and stalling. The
252 stalled ribosome on *msrDL* covers the first half of the hairpin of the RIT and therefore prevents
253 its formation and transcription termination (**Figure 2C** and **S3**).

254 The main dissimilarity between tested macrolides resides mainly in the presence or
255 absence of a cladinose moiety on C3 of the macrocyclic lactone ring which appears to be
256 critical for MsrDL-SRC formation (**Figure 3A**) similarly to ErmCL (Vazquez-Laslop et al., 2008).
257 Absence of significant toeprint in presence of TEL (whose C3 cladinose sugar is replaced by
258 a keto group) suggests that *msrDL* may be translated in this condition. TYL and SPI differ from
259 the other macrolides by the presence of disaccharide mycaminose-mycarose in place of the
260 C5 monosaccharide desosamine. When bound to the ribosome, this extended sugar moiety
261 protrudes into the PTC of the ribosome (Hansen et al., 2002). Absence of intermediate toeprint
262 and increase of the toeprint corresponding to initiation complex in presence of these two drugs

263 imply that these antibiotics stabilize the initiation complex. Previous results (Hansen et al.,
264 2002; Mao and Robishaw, 1971; Poulsen et al., 2000) have shown that they inhibit the
265 formation of the peptide bond, our result suggests that it occurs mainly for the first peptide
266 bond formation (**Figure 3A**).

267 We submitted the sequence of MsrDL to an alanine-scanning to investigate the
268 importance of each residue and their ability to induce *msrD*$_{(1\text{-}3)}$:*yfp* reporter, which indirectly
269 reports the formation of an ERY-dependent SRC. The scan shows a strong reduction of
270 inducibility for all the mutated residues with the exception Y2 (**Figure 3D**). Since MsrDL is a
271 hexapeptide, it is evident that most of the amino acids would have their importance to maintain
272 a conformation able to sense ERY. A complete loss of inducibility has been observed for
273 residues L3 and I4 suggesting that these two residues were directly involved in drug-sensing,
274 which was structurally confirmed and detailed in the next section (**Figure 4**). Moreover,
275 considering that MsrDL inhibits the action of both RF1/RF2 in presence of ERY, we mutated
276 UAA stop codon into RF1-specific UAG and RF2-specific UGA stop codons to investigate a
277 putative preferential inhibition as previously shown for TnaC (Emmanuel et al., 2019). Mutation
278 of UAA into UAG or UGA reduces the level of inducibility of the reporter gene (**Figure 3E**),
279 demonstrating a better expression of the reporter gene when both RF1 and RF2 are inhibited
280 compared to situations where RF1 or RF2 are inhibited separately. This observation is
281 corroborated by our phylogenetic analysis which revealed a large prevalence of UAA stop
282 codon among the different *msrDL* variants (**Figure S2A**). Most likely the UAA stop codon has
283 been selected by evolution to maximize *msrD* expression in presence of an inducer.

284

285 **Molecular mechanism of ribosome stalling by MsrDL**

286 To understand how MsrDL inhibits translation termination in presence of ERY, a
287 synthetic mRNA containing a single *msrDL* copy was translated *in vitro* with purified *E. coli*
288 DB10 ribosomes in presence of ERY as described in **Figure S4A** and the resulting sample
289 was subjected to cryo-EM. Single-particle reconstruction of MsrDL-SRC was done by refining
290 two subclasses, one containing only P-tRNAS and one containing P/E-tRNAs (respectively

291 11% and 28.1% of total particles), as described in methods and on **Figure S4B**. It resulted an
292 initial map of 70S ribosome (EMD-13805) with an average resolution of 3.0 Å that was
293 subjected to multibody refinement, generating reconstructions for the body and the head of the
294 small subunit (EMD-13807 and EMD-13808) and the large subunit (EMD-13806), presenting
295 average resolutions of 3.08, 3.3 and 2.97 Å, respectively (**Figures S4B** and **C**). The resolutions
296 of the derived reconstructions were consistent with clear and unambiguous assignment of
297 ribosomal proteins side chains, rRNA nucleotides and some post-transcriptional modifications
298 (**Figures S4D, E** and **F**). Local resolution of the codon-anticodon allowed unambiguous
299 identification of the P tRNA as an elongator $_{Met}$tRNA^{Met} (**Figure S4E**), which is also confirmed
300 by the presence of distinctive elements such as N4-acetylcytidine at position 34 (ac^{4}C34) and
301 N6-threonylcarbamoyladenosine at position 37 (t^{6}A37) (**Figures S4E** and **F**) (Ohashi et al.,
302 1972; Varshney et al., 1993), consistently with the toeprint results which assigned the M6
303 codon in the P site and UAA stop codon in the A site (**Figure 3C**).

304 A clear density corresponding to ERY bound in its canonical position was found at the
305 entrance of the NPET (**Figures 4A**, **4B** and **S4D**), allowing unambiguous attribution of
306 macrocyclic lactone ring, cladinose and desosamine sugars. A continuous density at the 3'
307 end of P tRNA extending within the entrance of ribosome tunnel was identified as MsrDL-NC
308 and local resolution of ~3 Å allowed to model the peptide *de novo* (**Figure 4B** and **S4D**). It
309 adopts a hook-like shape with its C-terminal extremity protruding into a cavity at the entrance
310 of the tunnel delimited by 23S rRNA nucleotides U2584, U2586, G2608 and C2610 (**Figure**
311 **4B**). One noticeable feature of MsrDL interaction with the ribosome is its residue Y2 that budge
312 out the base U2584 to form a π-stacking with the base G2583 (**Figures 4C** and **D**) in place of
313 the U2584. This unique interaction should stabilize the peptide conformation, while it appears
314 structurally significant, it is not strictly essential since replacement of the Y2 by an alanine
315 reduces by less than 50% the induction of the reporter gene (**Figure 3D**). In addition, the Y2
316 is substituted in some MsrDL variants (**Figure S2A**). MsrDL does not show numerous
317 significant electrostatic interactions with the ribosome since it is mostly composed of
318 hydrophobic amino acids. It is likely stabilized by hydrophobic interactions.

319 Our biochemical investigations showed that MsrDL-SRC were formed due to hampered
320 translation termination on UAA stop codon. This stop codon is recognized by RF1 and RF2
321 which subsequently catalyze peptide hydrolysis via their conserved GGQ motif protruding
322 within the PTC. Structural alignment of our model to RF1- and RF2-containing ribosome
323 structures (Pierson et al., 2016) revealed that proper accommodation of the RFs is prevented
324 by steric clashes of the methylated glutamine and the following glycines of the GGQ motif with
325 the residue F5 of MsrDL and 23S rRNA bases U2584 and U2585 respectively (**Figure 4E**).
326 The conformation of MsrDL peptide stabilizes the PTC in an uninduced conformation rather
327 than an induced one (Martin Schmeing et al., 2005) which catalyzes the peptide bond
328 formation (**Figure 4F**) as 23S rRNA base U2585 would clash with MsrDL. Structural alignment
329 of MsrDL-SRC with ErmBL- and ErmCL-SRC demonstrates that bases U2506 and 2585 are
330 not in the same conformation (**Figures S5A** and **B**), these bases in MsrDL-SRC being in a
331 conformation more similar to ErmDL-, SpeFL- and TnaC(R23F)-SRC (**Figures S5C** to **E**)
332 (Arenz et al., 2014a, 2016; Beckert et al., 2021; Herrero del Valle et al., 2020; van der Stel et
333 al., 2021). However, unusual position of base U2584 seems to be a unique feature of MsrDL-
334 SRC.

335 MsrDL may monitor the presence of cladinose-containing drugs as our *in vivo* and *in*
336 *vitro* experiments suggested. Mutation of residues L3 and I4 abolished induction of the reporter
337 gene suggesting that they were critical for drug recognition and/or conformation of the peptide
338 (**Figure 3D**). Consistently, in our model we identified residue L3 as the closest amino acid from
339 cladinose moiety and residue I4 as the closest from desosamine moiety (**Figure 4B** and **4G**).
340 However, similarly to ErmBL, no close contact between the nascent chain and the drug was
341 observed (Arenz et al., 2014b, 2016), residue L3 being ~3.8 Å away from cladinose sugar and
342 residue I4 being ~3.9 Å away from desosamine sugar, consistently with a hydrophobic
343 interaction between MsrDL and the drug (**Figures 4G** to **I**). This observation is also
344 corroborated by previous descriptions of pentapeptides conferring ERY resistance in which the
345 presence of a leucine or isoleucine at position 3 was critical for drug recognition (Lovmar et
346 al., 2006; Tenson et al., 1997). Moreover, the importance of 23S rRNA residue A2062 in acting

347 as an ERY-sensor and in contributing to silence the PTC, has been demonstrated for some
348 regulatory leader peptides (Koch et al., 2017; Vázquez-Laslop et al., 2010). In the case of
349 ErmCL, the critical feature for macrolide-dependent stalling is the rotation of the base A2062
350 that forms an Hoogsteen base pairing with m^2A2503 (Arenz et al., 2014a; Koch et al., 2017;
351 Vázquez-Laslop et al., 2010). The structure of MsrDL-SRC shows that residue I4 restraints
352 rotation of base A2062 (**Figure 4J**). Therefore, MsrDL induces an A2062/m^2A2503-
353 independent ribosome stalling (Vázquez-Laslop et al., 2010).

354 The path of MsrDL-NC within the ribosomal tunnel contrasts from all previous
355 descriptions of elongating polypeptides (**Figures 5A** to **5C**). Indeed, ERY-sensing ErmBL,
356 ErmCL and ErmDL leader peptides (Arenz et al., 2014a, 2016; Beckert et al., 2021) engage in
357 the NPET and go partially through ERY, while MsrDL curves before encountering the ligand
358 then engages into a dead-end crevice at the entrance of NPET (**Figures 4B** and **5B**). The
359 same observation (**Figure 5C**) can be made with metabolite-sensing SpeFL/TnaC(R23F)
360 leader peptides (Herrero del Valle et al., 2020; van der Stel et al., 2021). The first methionine
361 of MsrDL-NC latches into the dead-end crevice which is delimited by 23S rRNA nucleotides
362 U2584, U2586, G2608 and C2610 (**Figures 5A**, **5B** and **5C**). This crevice, named proximal
363 crevice, located at the base of helix 93 (h93) is part of domain V of 23S rRNA and is conserved
364 from bacteria to human mitoribosome and cytosolic ribosome (**Figures 5D**, **S5F** and **S5G**).

365

366 **MsrD negatively regulates its own expression**

367 MsrD protein provides antibiotic resistance by rescuing ERY-stalled ribosome while
368 *msrDL* translation in presence of ERY leads to the formation of a SRC. If MsrD is also able to
369 rescue this SRC, it will repress its own expression and form a feedback loop similarly to Vga(A)
370 (Vimberg et al., 2020). We tested this hypothesis using *E. coli* DB10 strains double transformed
371 with pMMB-*msrDL-msrD*$_{(1-3)}$:*yfp* and the compatible pBAD plasmid expressing various *msrD*
372 variants. Strains were grown in presence of ERY at 300 nM with their optical density and
373 fluorescence monitored (**Figure 6A**). Strain carrying the pBAD-*control* showed high
374 fluorescence and low OD_{600} as observed in **Figure 2A,** reflecting an induction of the reporter

375 and a susceptibility to ERY. On the contrary, expression of *msrD* led to higher cell growth and
376 a strong reduction of fluorescence which correspond respectively to antibiotic resistance and
377 repression of the expression of the reporter. These results support that MsrD can rescue
378 MsrDL-SRC and therefore releases the RIT repressing *msrD* transcription.

379 The strain expressing $msrD_{E125Q}$ has a low ERY resistance (**Figure 1F**). When it is co-
380 transformed with the pMMB-$msrDL\text{-}msrD_{(1\text{-}3)}$:*yfp* plasmid, no resistance is observed, possibly
381 because the presence of the two plasmid creates some toxicity. Overall, the results show that
382 MsrD variants that lost the ability to provide antibiotic resistance (ΔPtIM, ΔLoop and ATPase
383 deficient mutants) also lost the ability to rescue MsrDL-SRC (**Figure 6A**). Point mutations in
384 the Loop of the PtIM indicated some discrepancy between antibiotic resistance phenotype and
385 MsrDL-SRC rescue. All the mutants show an intermediary phenotype with less antibiotic
386 resistance and less repression of reporter compared to MsrD. The mutant $MsrD_{H244w}$ has the
387 same repression effect on the reporter than $MsrD_{H244A}$ for an equivalent OD_{600} but it provides
388 more that 3 times less antibiotic resistance (**Figures 1H** and **6A**). The mutant $MsrD_{R241A}$ which
389 provides a resistance close to MsrD does not rescue the MsrDL-SRC as efficiently as the latter
390 one (**Figures 1H** and **6A**). Mutants $MsrD_{L242A}$ and $MsrD_{H244A}$ provide similar resistance, but
391 $MsrD_{H244A}$ confers a stronger repression of the reporter (**Figures 1H** and **6A**). Together these
392 observations demonstrate that the determinants of the dual function of MsrD in conferring
393 antibiotic resistance and rescuing MsrDL-SRC are overall similar.

394

395 **DISCUSSION**

396 We used genetic, molecular biology and structural approaches to dissect the regulation
397 of the ARE ABC-F MsrD, its effect on ERY-stalled ribosomes and to provide information on
398 ARE ABC-F mechanisms of action that were lacking to date despite structural investigations
399 (Crowe-McAuliffe et al., 2018, 2021; Su et al., 2018). We characterized the *msrDL* regulatory
400 ORF which inhibits its own translation termination in presence of ribosome-bound cladinose-
401 containing macrolides (**Figures 3, 4 and 6B**). Our structural data show that this inhibition
402 results from the conjoint effects of: (*i*) MsrDL maintaining 23S rRNA bases U2506 and U2585

403 in an uninduced conformation (**Figure 4F**), (*ii*) the steric occlusion by U2584, U2585 and
404 MsrDL residue F5 that precludes the productive accommodation of RF1/RF2 (**Figure 3C** and
405 **4E**). MsrDL-stalled ribosome then hampers formation of a RIT allowing transcription of *msrD*
406 (**Figures 2C, 3A, 3C** and **6B**).

407 MsrD can bind with some specificity to ERY-stalled ribosome in an ATP-bound
408 conformation (**Figures 1D** and **1E**) and then its ATPase activity drives mechanical
409 rearrangements to rescue stalled ribosome. The ATPase mechanism that allows the rescue is
410 still unknown for ARE ABC-Fs and all the current structures of an ARE ABC-F in complex with
411 the ribosome were generated with an ATPase-dead mutant (Crowe-McAuliffe et al., 2018,
412 2021) or use of non-hydrolysable ATP analogues (Su et al., 2018). These structures do not
413 capture an antibiotic staled complex and embodies a reaction intermediary before or after
414 antibiotic release of an ARE ABC-F trapped on the ribosome. We provide here some evidence
415 about possible mechanisms (**Figure 6B**). We show that only one active ATPase site (Site II)
416 can provide some antibiotic resistance (**Figures 1F**) while the mutation inactivating Site I
417 generates a strong toxicity for the cell independently of the antibiotic (growth reduced by 70
418 %, **Figures 1F**). This suggests that even if Site II is used for antibiotic resistance mechanism,
419 it is also necessary for MsrD dissociation from the ribosome. The mutant of Site II shows a
420 stronger toxicity (growth reduced by 80 %, **Figures 1F**) and no antibiotic resistance, effects
421 related to less dissociation from the ribosome, Site I is therefore key for the release of MsrD.
422 Unexpectedly, mutation of the 2 sites leads to the same toxicity as for Site I (**Figures 1F**),
423 suggesting that having only Site I mutated induces a new MsrD conformation that inhibits the
424 ribosome further.

425 Results of polyribosomes experiments (**Figure 1C** to **E**, **Figure S1C**) suggest that MsrD
426 rescues stalled ribosomes by disassembling the two subunits. However, without an *in vitro*
427 assay that has been impeded by the low solubility of purified MsrD, we were not able to confirm
428 this observation. We envision two putative non-exclusive scenarios that involve for the first
429 one, a disassembling of ERY-stalled ribosomes, and for the other one, a displacement of the
430 drug followed by a restart of the translation process (**Figure 6B**). In one case or the other,

431 direct drug displacement by the factor seems excluded (**Figure S1E**). A key point for future
432 studies will be to explore the ATPase activity of MsrD in a stalled-ribosome context to
433 determine how many rounds of ATP hydrolysis are necessary to rescue the latter one. The
434 dissociation model requires the hydrolysis of only two ATP molecules, while antibiotic
435 displacement may require multiple hydrolysis rounds in Site II to displace the drug and to
436 position back the elongating peptide in a correct conformation in the NPET. So far, those
437 experiments have been challenging due to the low solubility of all the ARE ABC-F proteins
438 (Crowe-McAuliffe et al., 2021; Sharkey et al., 2016).

439 Alongside with ErmBL, ErmCL and ErmDL, MsrDL constitutes the fourth ERY-sensing
440 NC structurally described, however mechanisms of drug-sensing and PTC silencing greatly
441 differ. First, similarly to ErmCL, the presence of C3 cladinose sugar is required for stalling
442 (**Figures 3A** and **3B**) contrary to ErmBL and ErmDL that senses drugs lacking this moiety such
443 as oleandomycin, solithromycin or telithromycin (Arenz et al., 2014b; Beckert et al., 2021).
444 Second, similarly to ErmBL, no close contact between the drug and MsrDL was observed
445 (**Figures 4H** and **4I**) (Arenz et al., 2014b). Third, MsrDL is the only described leader peptide
446 that employs inhibition of its hydrolysis by RFs to induce stalling in presence of antibiotic,
447 similarly to the metabolite sensors TnaC and SpeFL (Herrero del Valle et al., 2020; van der
448 Stel et al., 2021). On the contrary, ErmBL (Arenz et al., 2016), ErmCL (Arenz et al., 2014a)
449 and ErmDL (Beckert et al., 2021) employ elongation inhibition. Fourth, ERY-dependent stalling
450 on *msrDL* regulates downstream *msrD* via transcriptional attenuation (**Figure 2B** and **2C**) while
451 it relies on translational attenuation for ErmBL, ErmCL and ErmDL (Arenz et al., 2014b;
452 Beckert et al., 2021; Mayford and Weisblum, 1989). Finally, MsrDL-NC conformation and path
453 within the ribosome greatly differ from previously described ligand-sensing leader peptides that
454 elongate within the tunnel (**Figures 5B** and **5C**) (Arenz et al., 2014a, 2016; Beckert et al.,
455 2021; Herrero del Valle et al., 2020; van der Stel et al., 2021). It adopts a hook-like shape
456 possibly due to hydrophobic interactions with the drug (**Figures 4B, 4G** to **4H**), while its
457 initiating methionine engages in a dead-end crevice at the NPET entrance (**Figure 5**). To our
458 knowledge, this is the first description of this crevice, conserved in prokaryotes and eukaryotes

459 (**Figures S5F** and **S5G**), as a functional site within the ribosome. We propose to name it
460 proximal crevice and believe it may contribute to the design of new antimicrobial drugs.

461 Some pentapeptides are known to mediate ERY resistance (Tenson et al., 1997;
462 Vimberg et al., 2004) by a mechanism that allows the exclusion of the ribosomal bond ERY
463 (Lovmar et al., 2006) upon peptidyl-tRNA hydrolysis by release factors. Exclusion and
464 hydrolysis are reduced for equivalent hexapeptides and the precise molecular mechanism is
465 still unknown, though it has been proposed that they engage in a putative dead end (Lovmar
466 et al., 2006). Those peptides share common features with the MsrDL hexapeptide: the third
467 amino acid is Leu/Ile, the forth is a hydrophobic one and they modulate termination in presence
468 of ERY. Thus, we propose that they could use the same crevice as MsrDL to catalyze their
469 action on ERY.

470 ARE ABC-F genes tend to be transcriptionally regulated as illustrated by *msrD*, *vmlR*,
471 *vgaA* and *lmo0919* (Dar et al., 2016; Ohki et al., 2005; Vimberg et al., 2020). However, as
472 described in the introduction, *msrD* forms an operon with the efflux pump *mefA* (**Figure 1A**)
473 which is also regulated *via* ribosome-mediated transcriptional attenuation, translational stalling
474 occurring on *mefAL* (Chancey et al., 2015b). Therefore, *msrD* is under the dual-regulation of
475 two ERY-sensing leader peptides. One explanation for this redundancy may reside in the need
476 for the bacteria to tightly regulate *msrD* because of its toxicity. Expression of *msrD* in *E. coli*
477 DB10 led to a 20 % growth defect compared to control condition (**Figure 1F**) suggesting that
478 *msrD* expression has a fitness cost for the bacteria and can be beneficial only in presence of
479 antibiotic. The presence of two attenuators creates a double-lock system to avoid any basal
480 expression in absence of inducer; and the feedback a loop, a mechanism to express only a
481 minimal amount of MsrD. Thus, as long as MefA can export enough antibiotic to provide
482 resistance, *msrD* should be kept repressed. The fitness cost of the expression of ARE ABC-F
483 genes is possibly the Achilles heel of bacteria containing those genes and may be exploited to
484 fight antibiotic resistance. MsrD provides resistance to ERY, AZY and TEL but only the first
485 two induce its expression, indicating that MsrD can provide some resistance for an antibiotic

486 which does not induce its expression. Thus, MsrDL facilitates the use of MsrD by the bacteria
487 and maintains its evolution under its control.
488

ACKNOWLEDGMENTS

This work has benefited from the facilities and expertise of the Biophysical and Structural Chemistry platform (BPCS) at IECB, CNRS UMS3033, Inserm US001, University of Bordeaux. C.R.F. is funded by a doctoral grant from the french Ministère de l'Enseignement supérieur, de la Recherche et de l'Innovation, F.O. and G.B. have received support from the LABEX program (DYNAMO ANR-11-LABX-0011), and the ANR grants EZOtrad (ANR-14-ACHN-0027) for G.B. and ABC-F_AB (ANR-18-CE35-0010) for G.B. and Y.H., ERC-2017-STG #759120 "TransTryp" to Y.H. E.C.L. and C.A.I. have received funding for this project from the European Research Council (ERC) under the European Union's Horizon 2020 research and innovation program (Grant Agreement No. 724040). Authors would like to thank Dr. Olivier Chesneau (Département de Microbiologie, Institut Pasteur, Paris - France) for providing *E. coli* DB10 strain, plasmids pBAD33 and pVN50; Dr. Sylvain Durand and Dr. Maud Guillier (UMR 8261, CNRS, Université de Paris, Institut de Biologie Physico-Chimique, Paris - France) that kindly provided respectively bicyclomycin and equipment for toeprinting experiments. Authors would like also to thank Laura Monlezun and Tina Wang for proofreading the manuscript.

AUTHOR CONTRIBUTIONS

F.O. performed the first experiments that initiated the project. C.R.F. performed most of the experiments. S.N. performed northern blotting experiments. C.R.F. prepared the cryo-EM sample. H.S. prepared cryo-EM grids and imaged them. C.A.I. and Y.H. processed cryo-EM data. C.R.F and E.C.L. reconstructed the atomic model. G.B. initiated the project and designed the research program with Y.H. C.R.F. and G.B. wrote the paper with input from all authors.

DECLARATION OF INTERESTS

The authors declare no competing interests. Requests for materials should be addressed to G.B. (boel@ibpc.fr).

515 **MAIN FIGURE TITLES AND LEGENDS**

516 **Figure 1. Translation factor MsrD alleviates erythromycin effects upon translation *in***
517 ***vivo.*** (A) Organization of the *mefA/msrD* macrolide resistance operon. In presence of ERY,
518 ribosomes stall during translation of *mefAL* leading to transcription anti-attenuation, both *mefA*
519 and *msrD* being then transcribed. Similar mechanism occurs during translation of *msrDL*,
520 which regulates transcription of *msrD* only. (B) Sequence alignment of various *msr* homologs
521 visualized with Jalview according to percentage of identity. Positions of tested mutations are
522 highlighted in red and indicated by arrows. Main features of ABC-F proteins are indicated on
523 the schematic. Genebank accession numbers are indicated between brackets. See also
524 **Figure S1B**. (C, D and E) Polyribosomes analysis and western blotting of *E. coli* DB10
525 expressing *msrD* (pBAD-$msrD_{WT}$), $msrD_{EQ2}$ (pBAD-$msrD_{EQ2}$) or a control (pBAD-*Control*) in
526 presence or absence of ERY. "L" stands for lysate. See also **Figure S1C** and **S1D**. (F, G and
527 H) Relative growth of *E. coli* DB10 expressing *msrD* variants in presence of ERY after 24 h.
528 Optical densities were normalized relative to optical densities of *E. coli* DB10 pBAD-*Control*
529 grown in the absence of ERY. Error bars represent mean ± s.d. for triplicate experiments. See
530 also **Table S1**.

531

532 **Figure 2. Erythromycin-dependent transcriptional termination regulates *msrD***
533 **expression.** (A) ERY-dependent induction of $msrD_{(1\text{-}3)}$:*yfp*. Fluorescent reporters shown on
534 schematics have been introduced in *E. coli* DB10 and grew in presence of 1 mM IPTG and
535 increasing sublethal ERY concentrations during 17 h. Fluorescence has been plotted against
536 OD_{600}, error bars for both axes represent mean ± s.d. for triplicate experiments. (B) Northern
537 analysis of *msrD* transcript. RNAs were extracted before adding or not 1 mM IPTG ($T_{0'}$), 10
538 min after adding IPTG ($T_{10'}$), and 5, 15, 30, 60, 120 min after adding or not 100 nM ERY.
539 Location of probe in $msrD_{(1\text{-}3)}$:*yfp* 3' UTR is shown on **Figure 2A**. The presence of a second
540 band was also observed but we hypothesized that it was abortive transcript resulting from the
541 construct insofar as its presence correlates with induction by IPTG and ERY, and is no longer
542 detectable using other probes (data not shown). (C) Deletion of the intrinsic terminator between
543 *msrDL* and $msrD_{(1\text{-}3)}$:*yfp* leads to a constitutive induction in absence of ERY. Error bars for both
544 axes represent mean ± s.d. for triplicate experiments.

545

546 **Figure 3. MsrDL is a macrolide-sensing nascent chain inhibiting its translation**
547 **termination.** (A) Toeprinting assay of *msrDL* in the absence (-) or in the presence of 50 µM of
548 various macrolide antibiotics. Empty arrow indicates initiation codon. Plain arrows indicate
549 ribosome stalling. Chemical structure of antibiotics is shown, C3 cladinose sugar of ERY and
550 AZI being highlighted. See also **Figure S3**. (B) *In vivo* induction of $msrD_{(1:3)}$:*yfp* by various
551 PTC/NPET targeting antibiotics. Bacteria containing pMMB-*msrDL*-$msrD_{(1:3)}$:*yfp* were grown

552 during 17 h in presence of 1 mM IPTG, in the absence (grey histograms) or in the presence of
553 50 nM antibiotics (red histograms). Error bars represent mean ± s.d. for triplicate experiments.
554 (C) Toeprinting assay depleted of release factors was performed in the absence of ribosome
555 (line 1), in presence of 50 µM RTP to assess start codon (line 2), without or with 50 µM ERY
556 (line 3 and 4), without or with 50 µM ERY then supplemented with 100 µM puromycin (line 5
557 and 6), without or with 50 µM ERY in presence of RF1/RF2/RF3 (line 7 and 8). The schematic
558 indicates position of toe-printing signal on the synthetic mRNA, P site codon of MsrDL-SRC is
559 underlined. See also **Figure S3**. (D and E) Effects of *msrDL* variants on the expression of
560 $msrD_{(1:3)}$:*yfp*. Bacteria were grown during 17 h in presence of 1 mM IPTG, in the absence (grey
561 histograms) or in the presence of 100 nM ERY (red histograms). Error bars represent mean ±
562 s.d. for triplicate experiments.
563
564 **Figure 4. Structure of MsrDL-SRC.** (A) Transverse section of the cryo-EM map showing the
565 30S (grey) and 50S (white) ribosomal subunits, mRNA (purple), ERY (red) and MsrDL-NC
566 (gold) bound to P-site $tRNA^{Met}$ (beige). (B) Close-up of MsrDL-NC within ribosomal tunnel
567 showing experimental density and modelled structure, colored as **Figure 4A** while 23S rRNA
568 nucleotides are shown in light grey. (C-D) Presence of MsrDL residue Y2 displace nucleotide
569 U2584 out of its position when compared to RF1- (PDB 5J30, light blue) and RF2-containing
570 (PDB 5CZP, blue) termination complex, thus forming a π-stacking with G2583 (Pierson et al.,
571 2016). (E) Conformation of U2584 and U2585 prevent productive accommodation of RF1 (PDB
572 5J30, light blue) and RF2 (PDB 5CZP, blue) while catalytic methylated glutamine would clash
573 with MsrDL residue F5 (Pierson et al., 2016). (F) PTC in MsrDL-SRC (light grey) is stabilized
574 in an uninduced state (PDB 1VQ6, pink) rather than in an induced state (PDB 1VQN, green)
575 as U2585 is pushed back by MsrDL residue Y2 (Martin Schmeing et al., 2005). (G-I) Molecular
576 basis for C3 cladinose sugar recognition by MsrDL. Residue L3 is at proximity of cladinose
577 sugar while residue I4 is at proximity of desosamine sugar. TEL lacking cladinose sugar and
578 failing to form MsrDL-SRC has been aligned (PDB 4V7S) (Dunkle et al., 2010). (J) Presence
579 of residue I4 avoids rotation of A2062 to form an Hoogsteen base pairing with m^2A2503 as it
580 is the case for ErmCL-SRC (PDB 3J7Z, green) (Arenz et al., 2014a). Light blue dashed lines
581 indicate hydrogen bonds formed by Hoogsteen base pairing. For the whole figure, structures
582 were aligned on domain V of 23S rRNA. Spheres represent van der Waals radii.
583
584 **Figure 5. MsrDL engages in a conserved crevice at the NPET entrance.** (A) Secondary
585 structure of the *E. coli* 23S rRNA domain V showing location of the proximal crevice at the
586 base of h93. For the whole figure, nucleotides delimitating proximal crevice are shown in red.
587 (B-C) Comparison of MsrDL path (gold) with ERY-dependent leader peptides ErmBL (PDB
588 5JTE, blue), ErmCL (PDB 3J7Z, green), ErmDL (PDB 7NSO, teal) as well as L-ornithine-

589 sensing SpeFL (PDB 6TC3, pink) and L-tryptophan-sensing TnaC(R23F) (PDB 7O1A, purple)
590 (Arenz et al., 2014a, 2016; Beckert et al., 2021; Herrero del Valle et al., 2020; van der Stel et
591 al., 2021). See also **Figure S5A** to **S5E.** (D) Proximal crevice in domain V is conserved from
592 bacteria to human (MsrDL-SRC, grey; *S. aureus* PDB 6YEF, light green; *H. sapiens* 55S
593 mitoribosome PDB 7A5F, light blue; *H. sapiens* 80S ribosome PDB 6OLI, marine blue) (Desai
594 et al., 2020; Golubev et al., 2020; Li et al., 2019). See also **Figure S5G** and **S5F**. For the whole
595 figure, atomic model of MsrDL is shown with its experimental density. Structures were aligned
596 on domain V of 23S rRNA.
597
598 **Figure 6. MsrD negatively regulates its own synthesis upon erythromycin exposure.** (A)
599 Effects of MsrD variants on MsrDL. *E. coli* DB10 containing pMMB-*msrDL-msrD*(1-3)*:yfp* and
600 expressing various *msrD* mutants were grown in presence of 0.2 % L-Arabinose, 1 mM IPTG
601 and 300 nM ERY, both OD_{600} and fluorescence being recorded over 24 h. Fluorescence has
602 been plotted against OD_{600}, error bars for both axes represent mean ± s.d. for triplicate
603 experiments. Color code is same as **Figures 1F** to **1H**. Light green rectangle indicates bacterial
604 growth over control plasmid. (B) Model of MsrD regulating its own expression and providing
605 antibiotic resistance. In absence of ERY, RNAP drops off at Rho-independent transcription
606 terminator. In presence of ERY, the ribosome following the RNAP stalls and unwinds the
607 terminator leading to *msrD* transcription. Once translated, MsrD negatively regulates its own
608 expression on one side, and provides antibiotic resistance on the other side. ATP-bound MsrD
609 recognizes ERY-stalled ribosome and may either expel the antibiotic or dissociate the
610 ribosome, ATP site II being active. Activity in ATP site I leads to MsrD dissociation and
611 recycling.

612 **MAIN TABLE TITLES AND LEGENDS**

613 **Table 1. Minimum inhibitory concentration (MIC) and half maximal inhibitory**
614 **concentration (IC_{50}) of *E. coli* DB10 expressing *msrD* in presence of ribosome-targeting**
615 **antibiotics.** See methods for experimental details.

616

617 618

	pBAD-*Control*		pBAD-*msrD*$_{WT}$	
Antibiotic	**MIC (µM)**	**IC_{50} (µM)**	**MIC (µM)**	**IC_{50} (µM)**
Erythromycin	2	0,179 ± 0,007	16	4,592 ± 0,582
Azithromycin	0.25	0,046 ± 0,002	2	0,953 ± 0,053
Telithromycin	1	0,086 ± 0,008	2	0,714 ± 0,066
Tylosin	4	1,649 ± 0,151	4	1,672 ± 0,103
Spiramycin	2	0,758 ± 0,063	2	0,81 ± 0,078
Lincomycin	32	12,61 ± 2,154	32	12,62 ± 1,27
Linezolid	32	13,62 ± 2,064	32	13,41 ± 1,137
Retapamulin	1	0,071 ± 0,004	1	0,075 ± 0,007

619 **STAR METHODS**

620 KEY RESOURCES TABLE

REAGENT or RESOURCE	SOURCE	IDENTIFIER
Antibodies		
Anti-6xHis-tag (mouse - monoclonal)	Covalab	Cat# mab90001-P
Anti-mouse-HRP IgG (goat – polyclonal)	Covalab	Cat# Lab0252
Bacterial strains		
E. coli DB10 (Derived from *E. coli* PR7)	(Datta et al., 1974)	N/A
E. coli K12 MG1655	N/A	N/A
Chemicals, Peptides, and Recombinant Proteins		
[γ^{32}P]ATP 3000 Ci/mmol, 50 mCi/ml	Hartmann Analytic	Cat# SRP-301
Ampicillin	Euromedex	Cat# EU0400-D
Avian Myeloblastosis Virus Reverse Transcriptase	Promega	Cat# M5101
Azithromycin	SYNkinase	Cat# SYN-3010
Chloramphenicol	Euromedex	Cat# 3886-B
CloneAmp HiFi PCR Premix	Takara	Cat# 639298
ddNTPs	Sigma Aldrich	Cat# GE27-2045-01
dNTPs	New England Biolabs	Cat# N0447S
Erythromycin	Toku-E	Cat# E002-5G
Formamide Ultra High Purity	Electron Microscopy Sciences	Cat# 15745
Isopropyl β-D-1-thiogalactopyranoside	Euromedex	Cat# EU0008-C
K-Glutamate	Sigma Aldrich	Cat# 49601-100G
Lincomycin	Sigma Aldrich	Cat# 62143-1G
Linezolid	Sigma Aldrich	Cat# PZ0014-5MG
Mineral oil	Sigma Aldrich	Cat# M8410-1L
Mueller Hinton Broth	Sigma Aldrich	Cat# 70192-500G
NEBuilder HiFi DNA Assembly Master Mix	New England Biolabs	Cat# E2621L

Protease Inhibitor Cocktail	Sigma Aldrich	Cat# P8340-1ML
Puromycin	Sigma Aldrich	Cat# 540222-25MG
Putrescine	Sigma Aldrich	Cat# D13208-25G
Retapamulin	Sigma Aldrich	Cat# CDS023386-25MG
Spermidine	Sigma Aldrich	Cat# S2626-1G
Spiramycin	Sigma Aldrich	Cat# 46745-100MG
T4 Polynucleotide kinase	New England Biolabs	Cat# M0201L
T7 RiboMAX Large Scale RNA Production System	Promega	Cat# P1300
Taq DNA polymerase with ThermoPol Buffer	New England Biolabs	Cat# M0267S
Telithromycin	Sigma Aldrich	Cat# SML2162-5MG
THE Ambion RNA Storage Solution	Thermo Fisher Scientific	Cat# AM7000
TRIzol Reagent	Thermo Fisher Scientific	Cat# 15596026
Tylosin tartrate	Sigma Aldrich	Cat# 33847-250MG
ULTRAhyb-Oligo hydridization buffer	Thermo Fisher Scientific	Cat# AM8663
Critical commercial assays		
PURExpress 2.0	GeneFrontier	Cat# PF201-0.25-EX
PURExpress ΔRF123 kit	New England Biolabs	Cat# E6850S
PURExpress ΔRibosome kit	New England Biolabs	Cat# E3313S
Deposited data		
Atomic coordinates of erythromycin-stalled *Escherichia coli* 70S ribosome with streptococcal MsrDL nascent chain	This study	PDB 7Q4K
Cryo-EM maps of erythromycin-stalled *Escherichia coli* 70S ribosome with streptococcal MsrDL nascent chain	This study	EMD-13805, EMD-13806, EMD-13807, EMD-13808
Oligonucleotides		
See supplementary table 3	Eurofins Genomics	N/A

Recombinant DNA		
pBAD-*Control* (pBAD33)	(Nunez-Samudio and Chesneau, 2013)	N/A
pBAD-*msrD*$_{WT}$ (pVN50)	(Nunez-Samudio and Chesneau, 2013)	N/A
pBAD-*msrD*$_{EQ2}$	This study	N/A
pBAD-*msrD*$_{E125Q}$	This study	N/A
pBAD-*msrD*$_{E434Q}$	This study	N/A
pBAD-*msrD*$_{\Delta Loop}$	This study	N/A
pBAD-*msrD*$_{\Delta PtlM}$	This study	N/A
pBAD-*msrD*$_{R241A}$	This study	N/A
pBAD-*msrD*$_{L242A}$	This study	N/A
pBAD-*msrD*$_{H244A}$	This study	N/A
pBAD-*msrD*$_{H244W}$	This study	N/A
pMMB-67EH	(Fürste et al., 1986)	N/A
pMMB-67EH-*yfp*	This study	N/A
pMMBpLacO-67EH-*yfp*	This study	N/A
pMMB-*msrDL-msrD*$_{(1-3)}$*:yfp*	This study	N/A
pMMB-*msrDL*$_{(no_ORF)}$-*msrD*$_{(1-3)}$*:yfp*	This study	N/A
pMMB-*msrDL*$_{(no_term)}$-*msrD*$_{(1-3)}$*:yfp*	This study	N/A
pMMB-*msrDL*$_{(Y2A)}$-*msrD*$_{(1-3)}$*:yfp*	This study	N/A
pMMB-*msrDL*$_{(L3A)}$-*msrD*$_{(1-3)}$*:yfp*	This study	N/A
pMMB-*msrDL*$_{(I4A)}$-*msrD*$_{(1-3)}$*:yfp*	This study	N/A
pMMB-*msrDL*$_{(F5A)}$-*msrD*$_{(1-3)}$*:yfp*	This study	N/A
pMMB-*msrDL*$_{(M6A)}$-*msrD*$_{(1-3)}$*:yfp*	This study	N/A
pMMB-*msrDL*$_{(UAA>UGA)}$-*msrD*$_{(1-3)}$*:yfp*	This study	N/A
pMMB-*msrDL*$_{(UAA>UAG)}$-*msrD*$_{(1-3)}$*:yfp*	This study	N/A
Software and Algorithms		
ARNold	(Naville et al., 2011)	N/A

Clustal W	(Larkin et al., 2007)	N/A
Coot	(Emsley and Cowtan, 2004)	N/A
Fiji	(Schindelin et al., 2012)	N/A
Gctf	(Zhang, 2016)	N/A
Jalview	(Waterhouse et al., 2009)	N/A
MotionCor2	(Zheng et al., 2017)	N/A
Phenix	(Liebschner et al., 2019)	N/A
PRISM 7	GraphPad	N/A
PyMOL Molecular Graphics System	Schrödinger, Inc.	N/A
RELION 3	(Zivanov et al., 2018)	N/A
ResMap	(Kucukelbir et al., 2014)	N/A
SWISS-MODEL	(Waterhouse et al., 2018)	N/A
UCSF Chimera	(Pettersen et al., 2004)	N/A
UCSF ChimeraX	(Goddard et al., 2018)	N/A
Other		
Amersham Hybond-N+ Membrane	GE Healthcare	Cat# RPN203B
Biocomp Gradient Master	Biocomp Instruments	N/A
Biocomp Piston Gradient Fractionator	Biocomp Instruments	N/A
BMG ClarioStar	BMG Labtech	N/A
Clarity Western ECL Substrate	Bio-Rad	Cat# 170-5061
Direct-zol RNA Miniprep kit	Zymo Research	Cat# R2051
Immun-Blot PVDF Membranes for Protein Blotting	Bio-Rad	Cat# 1620177
Li-Cor Odyssey FC imaging system	Li-cor	N/A

QIAquick Nucleotide Removal kit	Qiagen	Cat# 28304
Storage Phosphor Screen BAS-IP MS 2040	Fujifilm	Cat# 28956474
Typhoon FLA 9500	GE Healthcare	N/A

621

622 **METHOD DETAILS**

623 **Construction of plasmids**

624 All strains and plasmids used in this study are listed in **key resources table**. Oligonucleotides
625 are listed in **supplementary table 3**. For the whole study, the considered reference sequence
626 for *mefA/msrD* macrolide resistance operon was a Tn916-type transposon inserted in
627 *Streptococcus pneumoniae* strain 23771 genome (Genbank accession number FR671415.1)
628 (Croucher et al., 2011). Plasmids pBAD-*Control* and pBAD-$msrD_{WT}$ containing a C-terminal
629 hexahistidine tag (originally referred as pBAD33 and pVN50) were kindly retrieved from Olivier
630 Chesneau at Institut Pasteur (Paris, France) (Nunez-Samudio and Chesneau, 2013). Both
631 *mefA/msrD* macrolide resistance operon and pBAD-$msrD_{WT}$ encode the same protein MsrD
632 (Uniprot accession number A0A496M710).

633

634 **pBAD plasmids**. Those plasmids allow a tight and stringent expression control via catabolite
635 repression, interest gene being repressed in presence of 0.4 % (w/v) β-D-Glucose and induced
636 in presence of 0.2 % (w/v) L-Arabinose. Transformed clones were selected with 20 $\mu g.ml^{-1}$
637 chloramphenicol. In this study, all *msrD* mutants contain a C-terminal hexahistidine tag.
638 Catalytic mutant $msrD_{EQ2}$ was generated by amplifying pBAD-$msrD_{WT}$ with primer pairs 5/6 and
639 7/8 (**Table S3**), both fragments being assembled with NEBuilder HiFi DNA Assembly Master
640 Mix (New England Biolabs). Catalytic mutants $msrD_{E125Q}$, $msrD_{E434Q}$ were generated via
641 quickchange mutagenesis with primers pairs 9/10 and 11/12. Mutants $msrD_{\Delta Loop}$ and $msrD_{\Delta PtIM}$
642 were generated based on phylogenetic alignments by deleting residues between K216/K254
643 and E189/A274 respectively, a three-glycine linker being added to allow flexibility, via
644 quickchange mutagenesis using primer pairs 13/14 and 15/16 (**Table S3**). Variants $msrD_{R241A}$,
645 $msrD_{L242A}$, $msrD_{H244A}$, $msrD_{H244W}$ were generated via fusion PCR by amplifying $msrD_{WT}$ with
646 primers pairs 1/18, 1/20, 1/22, 1/24 and 2/17, 2/19, 2/21, 2/23 respectively (**Table S3**).
647 Backbone was amplified with primer pair 3/4 and fragments were assembled with NEBuilder
648 HiFi DNA Assembly Master Mix (New England Biolabs).

649 **pMMB plasmids**. All pMMB constructs originated from a low copy IPTG-inducible plasmid
650 pMMB67EH-*yfp*, consisting in original pMMB67EH (Fürste et al., 1986) containing optimized
651 *venus-yfp* enhancing its translation under the control of P_{tac} promoter (manuscript in
652 preparation). Transformed clones were selected with 100 $\mu g.ml^{-1}$ ampicillin. To test *msrDL*
653 functions *in vivo*, several fluorescent reporter genes have been designed. First, pMMB67EH-
654 *yfp* native P_{tac} promoter was replaced by P_{LacO} promoter as previously described (Lutz and
655 Bujard, 1997):

656 5'- ATAAATGTGAGCGGATAACATTGACATTGTGAGCGGATAACAAGATACTGAGCAC**A** -
657 3' (lac operators, shaded grey; transcription start, bold). This IPTG-inducible promoter allows
658 a tight and stringent transcription regulation compared to P_{tac} promoter, insofar as no regulatory

659 element is found in the 5' UTR. Promoter was replaced by amplifying pMMB67EH-*yfp* with
660 primer pairs 25/26 (**Table S3**), PCR fragment being then re-circularized via NEBuilder HiFi
661 DNA Assembly Master Mix (New England Biolabs). Plasmid pMMB-*msrDL-msrD*$_{(1-3)}$*:yfp* has
662 been designed by introducing the sequence spanning from the first nucleotide downstream
663 *mefA* stop codon to *msrD* three first codons fused to *yfp*. The introduced sequence is as
664 follows: 5'-
665 ACAATATT**GGAGGA**ATATTTATGTATCTTATTTTCATGTAACTCTTCCTGCTAAAATCGCA
666 GGGTTTTCCCTGCATACAAGCAAATGAAAGCATGCGATTATAGACA**GGAGGA**AATGTTA
667 TGGAATTA-3' (RBS, bold; *msrDL*, shaded grey, *msrD* three first codons are underlined). To
668 clone such construct, *yfp* gene was amplified from pMMB67EH-*yfp* with primer pairs 27/29
669 then with 28/29 to generate the insert, backbone was amplified with primer pair 30/31 (**Table**
670 **S3**), both fragments being then assembled with NEBuilder HiFi DNA Assembly Master Mix
671 (New England Biolabs). Plasmid pMMB-*control* was built by removing the *msrDL-msrD*$_{(1-3)}$*:yfp*
672 cassette via quickchange mutagenesis using primer pair 32/33, the resulting construction
673 containing only the P_{LacO} promoter followed by the plasmid endogenous *rrnB* transcription
674 terminator. Plasmid pMMB-*msrDL*$_{(no_term)}$*-msrD*$_{(1-3)}$*:yfp (*where the RIT between *msrDL* and
675 *msrD* is deleted) was generated by amplifying pMMB-*msrDL-msrD*$_{(1-3)}$*:yfp* with primer pair
676 34/35, PCR fragment being then re-circularized via NEBuilder HiFi DNA Assembly Master Mix
677 (New England Biolabs). The various *msrDL* mutants were cloned via quickchange
678 mutagenesis by amplifying pMMB-*msrDL-msrD*$_{(1-3)}$*:yfp* with primers 36 to 51.
679

680 **Antibiotic susceptibility testing, MIC and IC50 determination**

681 A saturated preculture of *E. coli* DB10 transformed with pBAD plasmid was grown overnight at
682 37 °C under vigorous shaking in Luria-Bertani Miller broth (LB), 20 µg.ml^{-1} chloramphenicol
683 and supplemented with 0.4 % (w/v) β-D-Glucose. Antibiotic susceptibility testing assay was
684 performed in Mueller-Hinton broth (MH, Sigma Aldrich), antibiotics being diluted via serial
685 dilutions. A 96-wells flat-bottom plate (Flacon) was filled with a final volume per well of 200 µl,
686 containing 20 µg.ml^{-1} chloramphenicol and 0.2 % (w/v) L-Arabinose and antibiotic to test. Wells
687 were inoculated at OD_{600} ~0.03-0.04 prior to addition of 60 µl mineral oil (Sigma Aldrich)
688 avoiding evaporation but not oxygen diffusion. Plates were therefore incubated for 24 h in
689 CLARIOstar Plus plate reader (BMG Labtech) at 37 °C with 600 rpm double-orbital shaking,
690 OD_{600} being measured each 30 min. Optical densities at 24 h were then normalized relative to
691 optical densities of *E. coli* DB10 pBAD-*Control* grown in the absence of antibiotic in Prism 7
692 (GraphPad). MIC was determined as absence of growth compared to blank, IC50 was
693 calculated in Prism using equation Y=Bottom + (Top-
694 Bottom)/(1 + ((X^HillSlope)/(IC50^HillSlope))) and the standard deviation was calculated by
695 multiplying standard error by square root of n (n being at least 3 replicates). To generate

696 curves, for bacteria grown in absence of antibiotic (0 µM), since coordinates are plotted as
697 logarithms and since log(0) is undefined, this point has been approximated 2 log units below
698 the lowest tested value (*i.e.* 0.0625 µM) consistently with Prism user guide (Miller, 2003). Curve
699 fitting was performed with non-linear fitting function "log(inhibitor) vs. response -- Variable
700 slope" using Y=Bottom + (Top-Bottom)/(1+10^((LogIC50-X)*HillSlope)). Both equations gave
701 strictly the same result for IC_{50}.
702
703 ***In vivo* induction assay**
704 A saturated preculture of *E. coli* DB10 transformed with pMMB plasmid was grown overnight
705 at 37 °C under vigorous shaking in LB with 100 $\mu g.ml^{-1}$ ampicillin. For bacteria double-
706 transformed with pMMB and pBAD plasmids, media was also supplemented with 20 $\mu g.ml^{-1}$
707 chloramphenicol and supplemented with 0.4 % (w/v) β-D-Glucose. *In vivo* induction assay was
708 performed in Mueller-Hinton broth (MH, Sigma Aldrich). A 96-wells flat-bottom plate (Flacon)
709 was filled with a final volume per well of 200 µl, containing 100 $\mu g.ml^{-1}$ ampicillin, 1 mM
710 Isopropyl β-D-1-thiogalactopyranoside (IPTG). Growth medium was supplemented with 20
711 $\mu g.ml^{-1}$ chloramphenicol and 0.2 % (w/v) L-Arabinose if pBAD plasmid is present. Induction of
712 fluorescent reporters being antibiotic-dependent, growth media were supplemented with
713 required antibiotic accordingly. Plates were therefore incubated in CLARIOstar Plus plate
714 reader (BMG labtech) at 37 °C with 600 rpm double-orbital shaking up to 24 h, OD_{600} and
715 fluorescence (excitation: 497-15 nm, emission: 540-20 nm, gain 1600) being measured each
716 30 min.
717
718 **Polyribosomes fractionation**
719 Saturated precultures of *E. coli* DB10 transformed with pBAD-*control*, pBAD-$msrD_{WT}$ or pBAD-
720 $msrD_{EQ2}$ were grown overnight at 37 °C under vigorous shaking in LB, 20 $\mu g.ml^{-1}$
721 chloramphenicol, 0.4 % (w/v) β-D-Glucose. Growth media (MH, 20 $\mu g.ml^{-1}$ chloramphenicol,
722 0.2 % (w/v) L-Arabinose) was inoculated at OD_{600}=0.05 with normalized precultures, and cells
723 were grown at 37 °C and 180 rpm. When OD_{600}=0.5 was reached, cultures were splitted in two
724 and one half was treated with a 25 µM erythromycin. Cultures were then incubated 1 hour at
725 37 °C and 180 rpm before harvesting. Cultures were chilled and cells were harvested by
726 centrifuging 10 min at 8 000 rpm, 4 °C. Supernatant was discarded and cells were
727 resuspended in 350 µl of lysis buffer (20 mM Tris pH 8, 20 mM $MgCl_2$, 100 mM NH_4(OAc), 2
728 mM β-mercaptoethanol, 10 $mg.ml^{-1}$ lysozyme) and transferred in microtubes. Then, 30 µl of
729 sodium deoxycholate 10 % (w/v) was added and cells were mechanically lysed by 3 rounds of
730 freezing-thawing. Lysates were clarified by centrifuging 20 min at 18 000 xg, 4 °C and total
731 RNAs were quantified. Finally, 500 µg of total RNAs were loaded onto 10-40 % (w/v) sucrose
732 gradients (20 mM Tris pH 8, 20 mM $MgCl_2$, 100 mM NH_4(OAc), 2 mM β-mercaptoethanol) and

733 centrifuged 2 h at 40 000 rpm, 4 °C in SW41 rotor (Beckman Coulter). Samples were
734 fractionated and collected using Biocomp Piston Gradient Fractionator (BioComp
735 Instruments), absorbance being measured at 254 nm.
736
737 **Immunoblotting**
738 Fractions of 300 µl were precipitated overnight in 150 µg.ml^{-1} sodium deoxycholate and 15 %
739 trichloroacetic acid. Pellets were washed twice in cold acetone, dried and resuspended in 25
740 µl 1X Laemmli buffer, 10 µl being loaded on 12.5 % acrylamide SDS-PAGE gels. Concerning
741 total lysates, 10 µg of normalized total RNAs were loaded as control. Gels were resolved by
742 migrating at 0.04 A and then applied on Immun-Blot PVDF membrane (Bio-Rad) that had been
743 activated in absolute ethanol then washed in electro-transfer buffer (25 mM Tris base, 192 mM
744 glycine, 0.1 % (w/v) SDS, 10 % (v/v) absolute ethanol). Proteins were electro-transferred at
745 100 V during 1 h. Membranes were blocked by incubating 1 h in 1X PBS supplemented with
746 0.5 % nonfat dry milk then washed with 1X PBS. C-term His-tagged $MsrD_{WT}$ and $MsrD_{EQ2}$ were
747 detected using anti-6xHis-tag primary antibody (Covalab, 1:2 000 dilution in 1X PBS, 0.1 %
748 Tween-20) combined with anti-mouse-HRP secondary antibody (Covalab, 1:20 000 dilution in
749 1X PBS, 0.1 % Tween-20). Immunoblots were revealed by performing an ECL detection using
750 Clarity Western ECL Substrate (Bio-Rad) and imaged with Li-Cor Odyssey FC imaging system
751 (Li-Cor).
752
753 **Preparation of *E. coli* DB10 ribosomes**
754 An overnight saturated *E. coli* DB10 preculture was used to inoculate growth medium (LB,
755 dilution 1:100) and cells were grown at 37 °C and 180 rpm. When OD_{600}=0.5, cells were
756 washed and harvested by two centrifugations during 20 min, 5 000 xg at 4°C followed by
757 resuspensions in Buffer A (20 mM Tris pH 7.4, 10 mM Mg(OAc), 100 mM NH_4(OAc), 0.5 mM
758 EDTA). Pellets were resuspended in Buffer A supplemented with 6 mM β-mercaptoethanol,
759 10 mg.ml^{-1} lysozyme, 0.001 % (v/v) protease inhibitor cocktail (Sigma Aldrich) and lysed three
760 times at 2.5 kBar using a cell disrupter (Constant Systems Limited). Lysate was clarified by
761 two centrifugations during 15 min, 22 000 xg at 4°C then spun for 20 h, 34 700 rpm at 4 °C in
762 a Type 70 Ti rotor (Beckmann Coulter) through a 37.7 % (w/v) sucrose cushion in Buffer B (20
763 mM Tris pH 7.4, 10 mM Mg(OAc), 500 mM NH_4(OAc), 0.5 mM EDTA, 6 mM β-
764 mercaptoethanol). Sucrose cushions were decanted and ribosome pellets resuspended in
765 Buffer C (20 mM Tris pH 7.4, 7.5 mM Mg(OAc), 60 mM NH_4(OAc), 0.5 mM EDTA, 6 mM β-
766 mercaptoethanol). Finally, 12 mg of ribosomes were loaded onto 10-40 % (w/v) sucrose
767 gradients in Buffer C and centrifuged 18 h at 20 000 rpm, 4 °C in SW28 rotor (Beckman
768 Coulter). Gradients were fractionated using Biocomp Piston Gradient Fractionator (BioComp
769 Instruments), absorbance being measured at 254 nm. Fractions containing 70S ribosomes

770 were pooled, washed and concentrated in Amicon 50k (Merckmillipore) using Buffer C.
771 Ribosomes concentration was adjusted to 18-20 µM, then aliquoted and flash frozen in liquid
772 nitrogen.
773
774 **RNA extraction and northern blotting**
775 Total RNA extraction was realized using the RNAsnap method as previously described (Stead
776 et al., 2012). In brief, a preculture of *E. coli* DB10 containing pMMB-*msrDL-msrD*$_{(1-3)}$*:yfp* was
777 grown overnight at 37 °C under vigorous shaking in LB supplemented with 100 µg.ml^{-1}
778 ampicillin. Growth medium (MH, 100 µg.ml^{-1} ampicillin) was inoculated at OD_{600}=0.05, and
779 cells were grown at 37 °C and 180 rpm. When OD_{600}=0.5, cells were treated (or not) with 1
780 mM IPTG during 10 min, then treated (or not) with 100 nM erythromycin. Samples of 2 ml were
781 collected ($T_{0'}$ = before IPTG was added, $T_{10'}$= 10 min after IPTG was added, and 5 min, 15
782 min, 30 min, 60 min and 120 min after erythromycin was added), then spun during 1 min at
783 15 000 rpm. Growth media was removed and cells were resuspended in 100 µl RNAsnap
784 buffer (95 % (v/v) formamide, 18 mM EDTA, 0.025 % (v/v) SDS, 1 % (v/v) β-mercaptoethanol).
785 Samples were heated for 10 min at 95 °C then clarified by centrifuging 10 min, at 16 000 rpm
786 at 16 °C. For northern blotting analysis, 6 µg of total RNAs were resolved on a 1 % (w/v)
787 agarose gel then transferred onto Amersham Hybond-N+ Membrane (GE Healthcare) by
788 capillary transfer. Radioactive probe was prepared using 40 pmol of primer 55 and 5'-labelled
789 with 10 U of T4 Polynucleotide Kinase (New England Biolabs) and [γ^{32}P]ATP (150 µCi). Probe
790 was hybridized overnight at 42 °C using ULTRAhyb-Oligo hybridization buffer (Thermo Fisher
791 Scientific). Membrane was washed three times at 42 °C during 15 min (once in 2x SSC + 0.1
792 % (v/v) SDS, once in 1x SSC + 0.1 % (v/v) SDS and finally in 0.1x SSC + 0.1 % (v/v) SDS).
793 Radioactive signal was visualized by exposing 4 h a Storage Phosphor Screen BAS-IP MS
794 2040 (Fujifilm) then imaged with a Typhoon FLA 9500 (GE Healthcare).
795
796 ***In vitro* transcription**
797 *In vitro* transcription was carried out in T7 RiboMAX Large Scale RNA Production System kit
798 (Promega) according to manufacturer instructions. Briefly, to generate DNA matrix (**Table S4**),
799 T7 promoter (5'-GCGAATTAATACGACTCACTATAGGG-3') was added by PCR using primers
800 pair 52/53 (**Table S3**) and pMMB plasmids as templates. Transcription reactions were
801 incubated 4 h at 37 °C and transcripts were purified with TRIzol Reagent (Thermo Fisher
802 Scientific) and Direct-zol RNA Miniprep kit (Zymo Research), samples being eluted in THE
803 Ambion RNA Storage Solution (Thermo Fisher Scientific). Final concentration was adjusted to
804 5 pmol.µl^{-1}.

805 **Toeprinting assay**

806 Position of stalled ribosomes on mRNA was determined by toe-printing assay, slightly adapted
807 from previously described methods (Herrero del Valle et al., 2020; Seefeldt et al., 2015). *In*
808 *vitro* translation reactions were performed using PURExpress ΔRF123 kit and PURExpress
809 ΔRibosome (New England Biolabs) according to manufacturer instructions. Briefly, prior to *in*
810 *vitro* translation reactions, 0.5 µl of 500 µM ligand (e.g. erythromycin etc) was dried in a micro-
811 centrifuge tube, using a SpeedVac vacuum concentrator (Thermo Fisher Scientific), final
812 concentration being 50 µM once resuspended in a 5 µl reaction. Reactions were incubated
813 during 15 min at 37 °C using 5 pmol of RNA templates (generated as described above) and
814 3.3 µM of purified *E. coli* DB10 ribosomes. When needed, samples were treated with 100 µM
815 final puromycin and incubated 3 min more. Immediately, 2 pmol of CY5-labelled primer 54
816 complementary to NV1 sequence (Vazquez-Laslop et al., 2008) was added and incubated for
817 5 min at 37 °C. For each reaction, reverse transcription was performed with 0.5 µl
818 (corresponding to 5 U) of Avian Myeloblastosis Virus Reverse Transcriptase (Promega), 0.1
819 µl dNTP mix (10 mM), 0.4 µl Pure System Buffer (5 mM K-phosphate pH 7.3, 9 mM Mg(OAc),
820 95 mM K-glutamate, 5 mM NH_4Cl, 0.5 mM $CaCl_2$, 1 mM spermidine, 8 mM putrescine, 1 mM
821 DTT) and incubated 20 min at 37 °C. Reactions were quenched with 1 µl NaOH 5 M and
822 incubated 15 min at 37 °C. Alkali were therefore neutralized by adding 0.7 µl HCl 25%
823 immediately supplemented with 20 µl toe-printing resuspension buffer (300 mM Na(OAc) pH
824 5.5, 5 mM EDTA, 0.5% (v/v) SDS). Finally, cDNAs were purified using QIAquick Nucleotide
825 Removal kit (Qiagen), vacuum dried and resuspended in 6 µl formamide dye (95% (v/v)
826 formamide, 20 mM EDTA, 0.25% (w/v) bromophenol blue). Sanger sequencing was performed
827 on DNA matrix used for *in vitro* transcription. Briefly, each 20 µl reaction contained 7.5 nM DNA
828 matrix, 75 nM CY5-labelled primer 58, 40 µM of each dNTPs, 0.025 U Taq Pol (New England
829 Biolabds), 1x Thermo Pol Buffer (New England Biolabs) and corresponding ddNTPs (625 µM
830 ddCTP/ddTTP/ddATP or 50 µM ddGTP). After PCR, 20 µl formamide dye was added to each
831 sequencing reaction. Samples were denatured 3 min at 80 °C, then 5 µl of sequencing reaction
832 and 1.5 µl of toe-printing reaction were loaded on a 6% acrylamide/bis-acrylamide (19:1)
833 sequencing gel containing 8 M urea. Gel was resolved by migrating 90 min at 50 W, then
834 imaged using a Typhoon FLA 9500 (GE Healthcare Life Sciences) using CY5 mode, LPR Ch.2
835 filter and 635 nm laser.

836

837 **Preparation of MsrDL-SRC**

838 A DNA matrix (**Table S4**) was prepared with CloneAmp HiFi PCR Premix (Takara) using primer
839 pair 52/56 (**Table S3**) and plasmid pMMB-*msrDL-msrD*$_{(1-3)}$*:yfp* as matrix. The corresponding
840 mRNA was generated as described above. The complete sequence of MsrDL-SRC mRNA is:

5'- GGAGCGGAUAACAAGAUACUGAGCACAACAAUAUU**GGAGG**AAUAUUUAUGUAU CUUAUUUUCAUGUAACUCUUCCUGCUAAAAUCGCAGGGUUUUCCCUGC -3' (RBS, bold; *msrDL*, shaded grey; the ATG codon in the P site of stalled ribosomes is underlined). Prior to *in vitro* translation reaction, 1 µl of 500 µM erythromycin (50 µM final concentration once resuspended in 10 µl) has been dried in a micro-centrifuge tube, using a SpeedVac vacuum concentrator (Thermo Fisher Scientific). Dried erythromycin has been resuspended in a 10 µl *in vitro* translation reaction carried out in PURE*frex* 2.0 kit (Genefrontier), containing 1.83 µM of purified *E. coli* DB10 ribosomes and 3.6 µM mRNA (molar ratio 1:2). The reaction has been incubated for 10 minutes at 37 °C, before adding 100 µM final puromycin, and incubated 3 min more. Reaction was therefore diluted in ribosome purification Buffer C (20 mM Tris pH 7.4, 7.5 mM Mg(OAc), 60 mM NH_4(OAc), 0.5 mM EDTA, 6 mM β-mercaptoethanol) to reach a concentration of 150 nM ribosomes. Cryo-EM grids were immediately prepared.

Cryo-EM grids preparation

Safematic ccu-010 HV carbon coater was used to coat Quantifoil carbon grids (QF-R2/2-Cu) with a thin carbon layer of approximate thickness of 2nm. Grids were therefore glow discharged for 30 sec at 2 mA. Then, 4 µl of *in vitro* translation reaction diluted to 150 nM were applied, and after a 2 sec blotting (force 5) and 30 sec waiting time, grids were vitrified in liquid ethane using a Vitrobot Mark IV (FEI) set to 4 °C and 100 % humidity.

Image acquisition and processing

Data collection was performed on a Talos Arctica instrument (FEI Company) at 200 kV using the EPU software (Thermo Fisher Company) for automated data acquisition. Data were collected at a nominal under focus of -0.5 to -2.7 µm at a magnification of 120,000 X yielding a calibrated pixel size of 1.2 Å. Micrographs were recorded as movie stack on a K2 Summit direct electron detector (Gatan), each movie stack were fractionated into 65 frames for a total exposure of 6.5 sec corresponding to an electron dose of 64 $e^-/Å^2$. MotionCor2 (Zheng et al., 2017) was used for dose weighting, drift and whole-frame motion correction. A dose weighted average image of the whole stack was used to determine the contrast transfer function with the software Gctf (Zhang, 2016). Particles were picked using a Laplacian of gaussian function (min diameter 260 Å, max diameter 320 Å). A total of ~254k particles were extracted from a subset of motion-corrected images (1523 micrographs) presenting a resolution equal or better than 4 Å with a box size of 360 pixels. The particles were binned three folds for 2D and subsequent 3D classification. After 2 rounds of 2D classification in RELION 3 (Zivanov et al., 2018), ~158k particles were selected and submitted to Relion 3D classification (Zivanov et al., 2018). A classe of non-rotated 70S depicting high-resolution features and bearing a tRNA with various occupancies was selected, representing ~104k particles. This class was further 3D-

878 classified with a spherical mask engulfing the tRNAs binding sites (**Figure S4B**) into 4 classes,
879 thus yielding P/E-tRNAs, P-tRNA, A/P-tRNAs and E-tRNA -containg 70S reconstructions. Only
880 P-site containing reconstructions were used for further processing, which represents ~62k
881 particles displaying the same global conformation of the 70S. These particles where re-
882 extracted at the full pixel size (1.2 Å) and refined through the 3D auto-refinement performed in
883 RELION 3 (Zivanov et al., 2018) resulting in a 3Å reconstruction (**Figure S4C**), after CTF-
884 refinement, Bayesian particle polishing and post-processing in RELION 3. In spite of the
885 sufficient local resolution at the vicinity of MsrDL peptide at the PTC (~3Å), residual movements
886 of the 30S around the 50S can be deduced by the lower local resolutions of the head and the
887 body of the 30S. In order to improve their resolution so to derive a complete atomic model of
888 the entire 70S complex, we applied RELION 3 multi-body refinement by defining three bodies;
889 50S, 30S-head and 30S-body. After completion of the refinement, the reconstructions of the
890 30S-head, 30S-body and 50S reached average resolutions of 3.3, 3.08 and 2.97 Å,
891 respectively. The local resolution (**Figure S4B** and **D**) was estimated using ResMap
892 (Kucukelbir et al., 2014).
893
894 **Model building and refinement**
895 The atomic model of erythromycin-stalled *Escherichia coli* 70S ribosome with streptococcal
896 MsrDL nascent chain was built into cryo-EM maps using Coot and Phenix (Emsley and
897 Cowtan, 2004; Liebschner et al., 2019). Insofar as *E. coli* DB10 hasn't been sequenced yet,
898 we assumed that ribosomal proteins and rRNAs were strictly identical to *E. coli* K12.
899 Furthermore, we did not notice any significant features in the map. Structure of SpeFL-SRC in
900 response to L-ornithine was used as initial model (PDB 6TC3) (Herrero del Valle et al., 2020)
901 and has been fitted in 70S ribosome map EMD-13805. Then, each part of the ribosome (50S,
902 30S Body and 30S Head) has been individually inspected in the corresponding map
903 (respectively EMD-13806, EMD-13807 and EMD-13808), modified if necessary in Coot and
904 refined with Phenix. P-site elongator tRNA $_{Met}$tRNA^{Met} was modeled *de novo* based on *E. coli*
905 K12 MG1655 *metT* gene, posttranscriptional modifications were added consistently with
906 Modomics database (Boccaletto et al., 2018) (http://genesilico.pl/modomics/) and refined in
907 map. E-site tRNA $_{Phe}$tRNA^{Phe} was derived from crystal structure of phenylalanine tRNA from *E.*
908 *coli* (PDB 6Y3G) with minor adjustments (Bourgeois et al., 2020). Both tRNAs were refined in
909 Phenix using map EMD-13805. ERY, MsrDL leader peptide and mRNA were modeled *de novo*
910 and refined in the corresponding map.
911
912 **Figure preparation**
913 Growth curves, histograms and polyribosomes profiles were generated using GraphPad Prism
914 7 (GraphPad). Sequence alignments were visualized with JalView (Waterhouse et al., 2009).

915 Western blotting, northern blotting and toe-printing gels were analyzed using Fiji (Schindelin
916 et al., 2012). Figures depicting molecular structures or electronic density maps were prepared
917 using PyMOL Molecular Graphics System, Chimera and ChimeraX (Goddard et al., 2018;
918 Pettersen et al., 2004).
919
920 **Quantification and statistical analysis**
921 Statistical details can be found in the figure legends. Statistical significance was assessed
922 using unpaired t-Test function in Prism 7 (GraphPad).
923
924 **Data and software availability**
925 Cryo-EM map of erythromycin-stalled *Escherichia coli* 70S ribosome with streptococcal MsrDL
926 nascent chain has been deposited at the Electron Microscopy Data Bank (EMDB) with
927 accession code EMD-13805, as well as 50S, 30S Body and 30S Head maps obtained after
928 multibody refinement with accession code EMD-13806, EMD-13807, EMD-13808 respectively.
929 Corresponding atomic model has been deposited in the Protein Data Bank (PDB) with
930 accession code 7Q4K.
931

REFERENCES

Ambrose, K.D., Nisbet, R., and Stephens, D.S. (2005). Macrolide Efflux in Streptococcus pneumoniae Is Mediated by a Dual Efflux Pump (mel and mef) and Is Erythromycin Inducible. Antimicrob Agents Chemother *49*, 4203–4209.

Arenz, S., Meydan, S., Starosta, A.L., Berninghausen, O., Beckmann, R., Vázquez-Laslop, N., and Wilson, D.N. (2014a). Drug Sensing by the Ribosome Induces Translational Arrest via Active Site Perturbation. Molecular Cell *56*, 446–452.

Arenz, S., Ramu, H., Gupta, P., Berninghausen, O., Beckmann, R., Vázquez-Laslop, N., Mankin, A.S., and Wilson, D.N. (2014b). Molecular basis for erythromycin-dependent ribosome stalling during translation of the ErmBL leader peptide. Nature Communications *5*, 3501.

Arenz, S., Bock, L.V., Graf, M., Innis, C.A., Beckmann, R., Grubmüller, H., Vaiana, A.C., and Wilson, D.N. (2016). A combined cryo-EM and molecular dynamics approach reveals the mechanism of ErmBL-mediated translation arrest. Nat Commun *7*.

Bailey, M., Chettiath, T., and Mankin, A.S. (2008). Induction of erm(C) Expression by Noninducing Antibiotics. Antimicrob Agents Chemother *52*, 866–874.

Banerjee, S., Chalissery, J., Bandey, I., and Sen, R. (2006). Rho-dependent Transcription Termination: More Questions than Answers. J Microbiol *44*, 11–22.

Beckert, B., Leroy, E.C., Sothiselvam, S., Bock, L.V., Svetlov, M.S., Graf, M., Arenz, S., Abdelshahid, M., Seip, B., Grubmüller, H., et al. (2021). Structural and mechanistic basis for translation inhibition by macrolide and ketolide antibiotics. Nat Commun *12*, 4466.

de Block, T., Laumen, J.G.E., Van Dijck, C., Abdellati, S., De Baetselier, I., Manoharan-Basil, S.S., Van den Bossche, D., and Kenyon, C. (2021). WGS of Commensal Neisseria Reveals Acquisition of a New Ribosomal Protection Protein (MsrD) as a Possible Explanation for High Level Azithromycin Resistance in Belgium. Pathogens *10*, 384.

Boccaletto, P., Machnicka, M.A., Purta, E., Piątkowski, P., Bagiński, B., Wirecki, T.K., de Crécy-Lagard, V., Ross, R., Limbach, P.A., Kotter, A., et al. (2018). MODOMICS: a database of RNA modification pathways. 2017 update. Nucleic Acids Res *46*, D303–D307.

Boël, G., Smith, P.C., Ning, W., Englander, M.T., Chen, B., Hashem, Y., Testa, A.J., Fischer, J.J., Wieden, H.-J., Frank, J., et al. (2014). The ABC-F protein EttA gates ribosome entry into the translation elongation cycle. Nat Struct Mol Biol *21*, 143–151.

Bourgeois, G., Seguin, J., Babin, M., Gondry, M., Mechulam, Y., and Schmitt, E. (2020). Structural basis of the interaction between cyclodipeptide synthases and aminoacylated tRNA substrates. RNA *26*, 1589–1602.

Chancey, S.T., Agrawal, S., Schroeder, M.R., Farley, M.M., Tettelin, H., and Stephens, D.S. (2015a). Composite mobile genetic elements disseminating macrolide resistance in Streptococcus pneumoniae. Front. Microbiol. *6*.

Chancey, S.T., Bai, X., Kumar, N., Drabek, E.F., Daugherty, S.C., Colon, T., Ott, S., Sengamalay, N., Sadzewicz, L., Tallon, L.J., et al. (2015b). Transcriptional Attenuation Controls Macrolide Inducible Efflux and Resistance in Streptococcus pneumoniae and in Other Gram-Positive Bacteria Containing mef/mel(msr(D)) Elements. PLOS ONE *10*, e0116254.

Chen, B., Boël, G., Hashem, Y., Ning, W., Fei, J., Wang, C., Gonzalez, R.L., Hunt, J.F., and Frank, J. (2014). EttA regulates translation by binding the ribosomal E site and restricting ribosome-tRNA dynamics. Nat Struct Mol Biol *21*, 152–159.

Croucher, N.J., Harris, S.R., Fraser, C., Quail, M.A., Burton, J., van der Linden, M., McGee, L., von Gottberg, A., Song, J.H., Ko, K.S., et al. (2011). Rapid pneumococcal evolution in response to clinical interventions. Science *331*, 430–434.

Crowe-McAuliffe, C., Graf, M., Huter, P., Takada, H., Abdelshahid, M., Nováček, J., Murina, V., Atkinson, G.C., Hauryliuk, V., and Wilson, D.N. (2018). Structural basis for antibiotic resistance mediated by the Bacillus subtilis ABCF ATPase VmlR. PNAS *115*, 8978–8983.

Crowe-McAuliffe, C., Murina, V., Turnbull, K.J., Kasari, M., Mohamad, M., Polte, C., Takada, H., Vaitkevicius, K., Johansson, J., Ignatova, Z., et al. (2021). Structural basis of ABCF-mediated resistance to pleuromutilin, lincosamide, and streptogramin A antibiotics in Gram-positive pathogens. Nat Commun *12*, 3577.

Daly, M.M., Doktor, S., Flamm, R., and Shortridge, D. (2004). Characterization and Prevalence of MefA, MefE, and the Associated msr(D) Gene in Streptococcus pneumoniae Clinical Isolates. J Clin Microbiol *42*, 3570–3574.

Dar, D., Shamir, M., Mellin, J.R., Koutero, M., Stern-Ginossar, N., Cossart, P., and Sorek, R. (2016). Term-seq reveals abundant ribo-regulation of antibiotics resistance in bacteria. Science *352*, aad9822.

Datta, N., Hedges, R.W., Becker, D., and Davies, J. (1974). Plasmid-determined Fusidic Acid Resistance in the Enterobacteriaceae. Microbiology, *83*, 191–196.

Del Grosso, M., Scotto d'Abusco, A., Iannelli, F., Pozzi, G., and Pantosti, A. (2004). Tn2009, a Tn916-Like Element Containing mef(E) in Streptococcus pneumoniae. Antimicrob Agents Chemother *48*, 2037–2042.

Del Grosso, M., Camilli, R., Iannelli, F., Pozzi, G., and Pantosti, A. (2006). The mef(E)-Carrying Genetic Element (mega) of Streptococcus pneumoniae: Insertion Sites and Association with Other Genetic Elements. Antimicrob Agents Chemother *50*, 3361–3366.

Dersch, P., Khan, M.A., Mühlen, S., and Görke, B. (2017). Roles of Regulatory RNAs for Antibiotic Resistance in Bacteria and Their Potential Value as Novel Drug Targets. Front. Microbiol. *8*.

Desai, N., Yang, H., Chandrasekaran, V., Kazi, R., Minczuk, M., and Ramakrishnan, V. (2020). Elongational stalling activates mitoribosome-associated quality control. Science *370*, 1105–1110.

Dubnau, D. (1985). Induction of ermC requires translation of the leader peptide. EMBO J *4*, 533–537.

Dunkle, J.A., Xiong, L., Mankin, A.S., and Cate, J.H.D. (2010). Structures of the Escherichia coli ribosome with antibiotics bound near the peptidyl transferase center explain spectra of drug action. Proc Natl Acad Sci U S A *107*, 17152–17157.

Emmanuel, J.S., Sengupta, A., Gordon, E.R., Noble, J.T., and Cruz-Vera, L.R. (2019). The regulatory TnaC nascent peptide preferentially inhibits release factor 2-mediated hydrolysis of peptidyl-tRNA. J Biol Chem *294*, 19224–19235.

Emsley, P., and Cowtan, K. (2004). Coot: model-building tools for molecular graphics. Acta Cryst D *60*, 2126–2132.

Fostier, C.R., Monlezun, L., Ousalem, F., Singh, S., Hunt, J.F., and Boël, G. (2021). ABC-F translation factors: from antibiotic resistance to immune response. FEBS Letters *595*, 675–706.

1013 Fürste, J.P., Pansegrau, W., Frank, R., Blöcker, H., Scholz, P., Bagdasarian, M., and Lanka, E. (1986).
1014 Molecular cloning of the plasmid RP4 primase region in a multi-host-range tacP expression vector. Gene
1015 *48*, 119–131.

1016 Gay, K., and Stephens, D.S. (2001). Structure and Dissemination of a Chromosomal Insertion Element
1017 Encoding Macrolide Efflux in Streptococcus pneumoniae. The Journal of Infectious Diseases *184*, 56–
1018 65.

1019 Goddard, T.D., Huang, C.C., Meng, E.C., Pettersen, E.F., Couch, G.S., Morris, J.H., and Ferrin, T.E.
1020 (2018). UCSF ChimeraX: Meeting modern challenges in visualization and analysis. Protein Sci *27*, 14–
1021 25.

1022 Golubev, A., Fatkhullin, B., Khusainov, I., Jenner, L., Gabdulkhakov, A., Validov, S., Yusupova, G.,
1023 Yusupov, M., and Usachev, K. (2020). Cryo-EM structure of the ribosome functional complex of the
1024 human pathogen Staphylococcus aureus at 3.2 Å resolution. FEBS Letters *594*, 3551–3567.

1025 González-Zorn, B., Catalan, A., Escudero, J.A., Domínguez, L., Teshager, T., Porrero, C., and Moreno,
1026 M.A. (2005). Genetic basis for dissemination of armA. Journal of Antimicrobial Chemotherapy *56*, 583–
1027 585.

1028 Hansen, J.L., Ippolito, J.A., Ban, N., Nissen, P., Moore, P.B., and Steitz, T.A. (2002). The Structures of
1029 Four Macrolide Antibiotics Bound to the Large Ribosomal Subunit. Molecular Cell *10*, 117–128.

1030 Hartz, D., McPheeters, D.S., Traut, R., and Gold, L. (1988). Extension inhibition analysis of translation
1031 initiation complexes. In Methods in Enzymology, (Academic Press), pp. 419–425.

1032 Herrero del Valle, A., Seip, B., Cervera-Marzal, I., Sacheau, G., Seefeldt, A.C., and Innis, C.A. (2020).
1033 Ornithine capture by a translating ribosome controls bacterial polyamine synthesis. Nature
1034 Microbiology *5*, 554–561.

1035 Horinouchi, S., and Weisblum, B. (1980). Posttranscriptional modification of mRNA conformation:
1036 Mechanism that regulates erythromycin-induced resistance. PNAS *77*, 7079–7083.

1037 Iannelli, F., Santagati, M., Santoro, F., Oggioni, M.R., Stefani, S., and Pozzi, G. (2014). Nucleotide
1038 sequence of conjugative prophage Φ1207.3 (formerly Tn1207.3) carrying the mef(A)/msr(D) genes for
1039 efflux resistance to macrolides in Streptococcus pyogenes. Front Microbiol *5*.

1040 Ito, K., and Chiba, S. (2013). Arrest Peptides: Cis-Acting Modulators of Translation. Annu. Rev.
1041 Biochem. *82*, 171–202.

1042 Kirsch, D.R., and Lai, M.H. (1984). Regulation of a macrolide resistance-beta-galactosidase (ermC-
1043 lacZ) gene fusion in Escherichia coli. J Bacteriol *159*, 381–384.

1044 Koch, M., Willi, J., Pradère, U., Hall, J., and Polacek, N. (2017). Critical 23S rRNA interactions for
1045 macrolide-dependent ribosome stalling on the ErmCL nascent peptide chain. Nucleic Acids Res *45*,
1046 6717–6728.

1047 Kucukelbir, A., Sigworth, F.J., and Tagare, H.D. (2014). The Local Resolution of Cryo-EM Density
1048 Maps. Nat Methods *11*, 63–65.

1049 Larkin, M.A., Blackshields, G., Brown, N.P., Chenna, R., McGettigan, P.A., McWilliam, H., Valentin,
1050 F., Wallace, I.M., Wilm, A., Lopez, R., et al. (2007). Clustal W and Clustal X version 2.0.
1051 Bioinformatics *23*, 2947–2948.

1052 Li, W., Ward, F.R., McClure, K.F., Chang, S.T.-L., Montabana, E., Liras, S., Dullea, R.G., and Cate,
1053 J.H.D. (2019). Structural basis for selective stalling of human ribosome nascent chain complexes by a
1054 drug-like molecule. Nat Struct Mol Biol *26*, 501–509.

1055 Liebschner, D., Afonine, P.V., Baker, M.L., Bunkóczi, G., Chen, V.B., Croll, T.I., Hintze, B., Hung, L.-
1056 W., Jain, S., McCoy, A.J., et al. (2019). Macromolecular structure determination using X-rays, neutrons
1057 and electrons: recent developments in Phenix. Acta Cryst D *75*, 861–877.

1058 Lovmar, M., Nilsson, K., Vimberg, V., Tenson, T., Nervall, M., and Ehrenberg, M. (2006). The
1059 Molecular Mechanism of Peptide-mediated Erythromycin Resistance *. Journal of Biological Chemistry
1060 *281*, 6742–6750.

1061 Lu, C., Ye, T. lu, Zhu, G. xing, Feng, P. ying, Ma, H., Lu, R. biao, and Lai, W. (2010). Phenotypic and
1062 Genetic Characteristics of Macrolide and Lincosamide Resistant Ureaplasma urealyticum Isolated in
1063 Guangzhou, China. Curr Microbiol *61*, 44–49.

1064 Lutz, R., and Bujard, H. (1997). Independent and Tight Regulation of Transcriptional Units in
1065 Escherichia Coli Via the LacR/O, the TetR/O and AraC/I1-I2 Regulatory Elements. Nucleic Acids Res
1066 *25*, 1203–1210.

1067 Mao, J.C., and Robishaw, E.E. (1971). Effects of macrolides on peptide-bond formation and
1068 translocation. Biochemistry *10*, 2054–2061.

1069 Martin Schmeing, T., Huang, K.S., Strobel, S.A., and Steitz, T.A. (2005). An induced-fit mechanism to
1070 promote peptide bond formation and exclude hydrolysis of peptidyl-tRNA. Nature *438*, 520–524.

1071 Mayford, M., and Weisblum, B. (1989). Conformational alterations in the ermC transcript in vivo during
1072 induction. EMBO J *8*, 4307–4314.

1073 Meydan, S., Marks, J., Klepacki, D., Sharma, V., Baranov, P.V., Firth, A.E., Margus, T., Kefi, A.,
1074 Vázquez-Laslop, N., and Mankin, A.S. (2019). Retapamulin-Assisted Ribosome Profiling Reveals the
1075 Alternative Bacterial Proteome. Molecular Cell *74*, 481-493.e6.

1076 Miller, J.R. (2003). GraphPad Prism Version 4.0 Step-by-Step Examples (GraphPad Software Inc., San
1077 Diego).

1078 Murina, V., Kasari, M., Takada, H., Hinnu, M., Saha, C.K., Grimshaw, J.W., Seki, T., Reith, M., Putrinš,
1079 M., Tenson, T., et al. (2019). ABCF ATPases Involved in Protein Synthesis, Ribosome Assembly and
1080 Antibiotic Resistance: Structural and Functional Diversification across the Tree of Life. Journal of
1081 Molecular Biology *431*, 3568–3590.

1082 Muto, H., Nakatogawa, H., and Ito, K. (2006). Genetically Encoded but Nonpolypeptide Prolyl-tRNA
1083 Functions in the A Site for SecM-Mediated Ribosomal Stall. Molecular Cell *22*, 545–552.

1084 Narayanan, C.S., and Dubnau, D. (1985). Evidence for the translational attenuation model: ribosome-
1085 binding studies and structural analysis with an in vitro run-off transcript of ermC. Nucleic Acids Res
1086 *13*, 7307–7326.

1087 Naville, M., Ghuillot-Gaudeffroy, A., Marchais, A., and Gautheret, D. (2011). ARNold: A web tool for
1088 the prediction of Rho-independent transcription terminators. RNA Biology *8*, 11–13.

1089 Nikaido, H. (2009). Multidrug Resistance in Bacteria. Annual Review of Biochemistry *78*, 119–146.

1090 Nikaido, H., and Pagès, J.-M. (2012). Broad-specificity efflux pumps and their role in multidrug
1091 resistance of Gram-negative bacteria. FEMS Microbiol Rev *36*, 340–363.

Nunez-Samudio, V., and Chesneau, O. (2013). Functional interplay between the ATP binding cassette Msr(D) protein and the membrane facilitator superfamily Mef(E) transporter for macrolide resistance in Escherichia coli. Research in Microbiology *164*, 226–235.

Ohashi, Z., Murao, K., Yahagi, T., Von Minden, D.L., McCloskey, J.A., and Nishimura, S. (1972). Characterization of C+ located in the first position of the anticodon of Escherichia coli tRNAMet as N4-acetylcytidine. Biochimica et Biophysica Acta (BBA) - Nucleic Acids and Protein Synthesis *262*, 209–213.

Ohki, R., Tateno, K., Takizawa, T., Aiso, T., and Murata, M. (2005). Transcriptional Termination Control of a Novel ABC Transporter Gene Involved in Antibiotic Resistance in Bacillus subtilis. J Bacteriol *187*, 5946–5954.

Ousalem, F., Singh, S., Chesneau, O., Hunt, J.F., and Boël, G. (2019). ABC-F proteins in mRNA translation and antibiotic resistance. Research in Microbiology *170*, 435–447.

Pettersen, E.F., Goddard, T.D., Huang, C.C., Couch, G.S., Greenblatt, D.M., Meng, E.C., and Ferrin, T.E. (2004). UCSF Chimera—A visualization system for exploratory research and analysis. Journal of Computational Chemistry *25*, 1605–1612.

Pierson, W.E., Hoffer, E.D., Keedy, H.E., Simms, C.L., Dunham, C.M., and Zaher, H.S. (2016). Uniformity of Peptide Release Is Maintained by Methylation of Release Factors. Cell Reports *17*, 11–18.

Poulsen, S.M., Kofoed, C., and Vester, B. (2000). Inhibition of the ribosomal peptidyl transferase reaction by the mycarose moiety of the antibiotics carbomycin, spiramycin and tylosin1 1Edited by D. E. Draper. Journal of Molecular Biology *304*, 471–481.

Ramu, H., Mankin, A., and Vazquez-Laslop, N. (2009). Programmed drug-dependent ribosome stalling. Mol Microbiol *71*, 811–824.

Ray-Soni, A., Bellecourt, M.J., and Landick, R. (2016). Mechanisms of Bacterial Transcription Termination: All Good Things Must End. Annual Review of Biochemistry *85*, 319–347.

Roberts, M.C., Sutcliffe, J., Courvalin, P., Jensen, L.B., Rood, J., and Seppala, H. (1999). Nomenclature for Macrolide and Macrolide-Lincosamide-Streptogramin B Resistance Determinants. Antimicrob Agents Chemother *43*, 2823–2830.

Schindelin, J., Arganda-Carreras, I., Frise, E., Kaynig, V., Longair, M., Pietzsch, T., Preibisch, S., Rueden, C., Saalfeld, S., Schmid, B., et al. (2012). Fiji: an open-source platform for biological-image analysis. Nature Methods *9*, 676–682.

Seefeldt, A.C., Nguyen, F., Antunes, S., Pérébaskine, N., Graf, M., Arenz, S., Inampudi, K.K., Douat, C., Guichard, G., Wilson, D.N., et al. (2015). The proline-rich antimicrobial peptide Onc112 inhibits translation by blocking and destabilizing the initiation complex. Nature Structural & Molecular Biology *22*, 470–475.

Seip, B., and Innis, C.A. (2016). How Widespread is Metabolite Sensing by Ribosome-Arresting Nascent Peptides? Journal of Molecular Biology *428*, 2217–2227.

Sharkey, L.K.R., Edwards, T.A., and O'Neill, A.J. (2016). ABC-F Proteins Mediate Antibiotic Resistance through Ribosomal Protection. MBio *7*.

Sharma, P., Gupta, S.K., Barrett, J.B., Hiott, L.M., Woodley, T.A., Kariyawasam, S., Frye, J.G., and Jackson, C.R. (2020). Comparison of Antimicrobial Resistance and Pan-Genome of Clinical and Non-Clinical Enterococcus cecorum from Poultry Using Whole-Genome Sequencing. Foods *9*, 686.

1134 Shimizu, Y., Inoue, A., Tomari, Y., Suzuki, T., Yokogawa, T., Nishikawa, K., and Ueda, T. (2001).
1135 Cell-free translation reconstituted with purified components. Nat Biotechnol *19*, 751–755.

1136 Siibak, T., Peil, L., Xiong, L., Mankin, A., Remme, J., and Tenson, T. (2009). Erythromycin- and
1137 Chloramphenicol-Induced Ribosomal Assembly Defects Are Secondary Effects of Protein Synthesis
1138 Inhibition. Antimicrobial Agents and Chemotherapy *53*, 563–571.

1139 Sothiselvam, S., Liu, B., Han, W., Ramu, H., Klepacki, D., Atkinson, G.C., Brauer, A., Remm, M.,
1140 Tenson, T., Schulten, K., et al. (2014). Macrolide antibiotics allosterically predispose the ribosome for
1141 translation arrest. Proc Natl Acad Sci U S A *111*, 9804–9809.

1142 Stead, M.B., Agrawal, A., Bowden, K.E., Nasir, R., Mohanty, B.K., Meagher, R.B., and Kushner, S.R.
1143 (2012). RNAsnap^{TM}: a rapid, quantitative and inexpensive, method for isolating total RNA from
1144 bacteria. Nucleic Acids Res *40*, e156.

1145 van der Stel, A.-X., Gordon, E.R., Sengupta, A., Martínez, A.K., Klepacki, D., Perry, T.N., Herrero del
1146 Valle, A., Vázquez-Laslop, N., Sachs, M.S., Cruz-Vera, L.R., et al. (2021). Structural basis for the
1147 tryptophan sensitivity of TnaC-mediated ribosome stalling. Nat Commun *12*, 5340.

1148 Su, W., Kumar, V., Ding, Y., Ero, R., Serra, A., Lee, B.S.T., Wong, A.S.W., Shi, J., Sze, S.K., Yang,
1149 L., et al. (2018). Ribosome protection by antibiotic resistance ATP-binding cassette protein. PNAS *115*,
1150 5157–5162.

1151 Tatsuno, I., Isaka, M., Masuno, K., Hata, N., Matsumoto, M., and Hasegawa, T. (2018). Functional
1152 Predominance of msr(D), Which Is More Effective as mef(A)-Associated Than mef(E)-Associated,
1153 Over mef(A)/mef(E) in Macrolide Resistance in Streptococcus pyogenes. Microbial Drug Resistance
1154 *24*, 1089–1097.

1155 Tenson, T., Xiong, L., Kloss, P., and Mankin, A.S. (1997). Erythromycin Resistance Peptides Selected
1156 from Random Peptide Libraries*. Journal of Biological Chemistry *272*, 17425–17430.

1157 Varshney, U., Lee, C.P., and RajBhandary, U.L. (1993). From elongator tRNA to initiator tRNA. PNAS
1158 *90*, 2305–2309.

1159 Vazquez-Laslop, N., Thum, C., and Mankin, A.S. (2008). Molecular Mechanism of Drug-Dependent
1160 Ribosome Stalling. Molecular Cell *30*, 190–202.

1161 Vázquez-Laslop, N., Ramu, H., Klepacki, D., Kannan, K., and Mankin, A.S. (2010). The key function
1162 of a conserved and modified rRNA residue in the ribosomal response to the nascent peptide. EMBO J
1163 *29*, 3108–3117.

1164 Vimberg, V., Xiong, L., Bailey, M., Tenson, T., and Mankin, A. (2004). Peptide-mediated macrolide
1165 resistance reveals possible specific interactions in the nascent peptide exit tunnel. Molecular
1166 Microbiology *54*, 376–385.

1167 Vimberg, V., Cavanagh, J.P., Novotna, M., Lenart, J., Ngoc, B.N.T., Vesela, J., Pain, M., Koberska, M.,
1168 and Novotna, G.B. (2020). Ribosome-Mediated Attenuation of vga(A) Expression Is Shaped by the
1169 Antibiotic Resistance Specificity of Vga(A) Protein Variants. Antimicrobial Agents and Chemotherapy
1170 *64*.

1171 Waterhouse, A., Bertoni, M., Bienert, S., Studer, G., Tauriello, G., Gumienny, R., Heer, F.T., de Beer,
1172 T.A.P., Rempfer, C., Bordoli, L., et al. (2018). SWISS-MODEL: homology modelling of protein
1173 structures and complexes. Nucleic Acids Res *46*, W296–W303.

1174 Waterhouse, A.M., Procter, J.B., Martin, D.M.A., Clamp, M., and Barton, G.J. (2009). Jalview Version
1175 2—a multiple sequence alignment editor and analysis workbench. Bioinformatics *25*, 1189–1191.

1176 Weisblum, B., Siddhikol, C., Lai, C.J., and Demohn, V. (1971). Erythromycin-Inducible Resistance in
1177 Staphylococcus aureus: Requirements for Induction. Journal of Bacteriology *106*, 835–847.

1178 Zhang, K. (2016). Gctf: Real-time CTF determination and correction. J Struct Biol *193*, 1–12.

1179 Zhang, Y., Tatsuno, I., Okada, R., Hata, N., Matsumoto, M., Isaka, M., Isobe, K.-I., and Hasegawa, T.
1180 (2016). Predominant role of msr(D) over mef(A) in macrolide resistance in Streptococcus pyogenes.
1181 Microbiology (Reading) *162*, 46–52.

1182 Zheng, S.Q., Palovcak, E., Armache, J.-P., Verba, K.A., Cheng, Y., and Agard, D.A. (2017).
1183 MotionCor2 - anisotropic correction of beam-induced motion for improved cryo-electron microscopy.
1184 Nat Methods *14*, 331–332.

1185 Zivanov, J., Nakane, T., Forsberg, B.O., Kimanius, D., Hagen, W.J., Lindahl, E., and Scheres, S.H.
1186 (2018). New tools for automated high-resolution cryo-EM structure determination in RELION-3. ELife
1187 *7*, e42166.

1188

1189

FIGURE 1

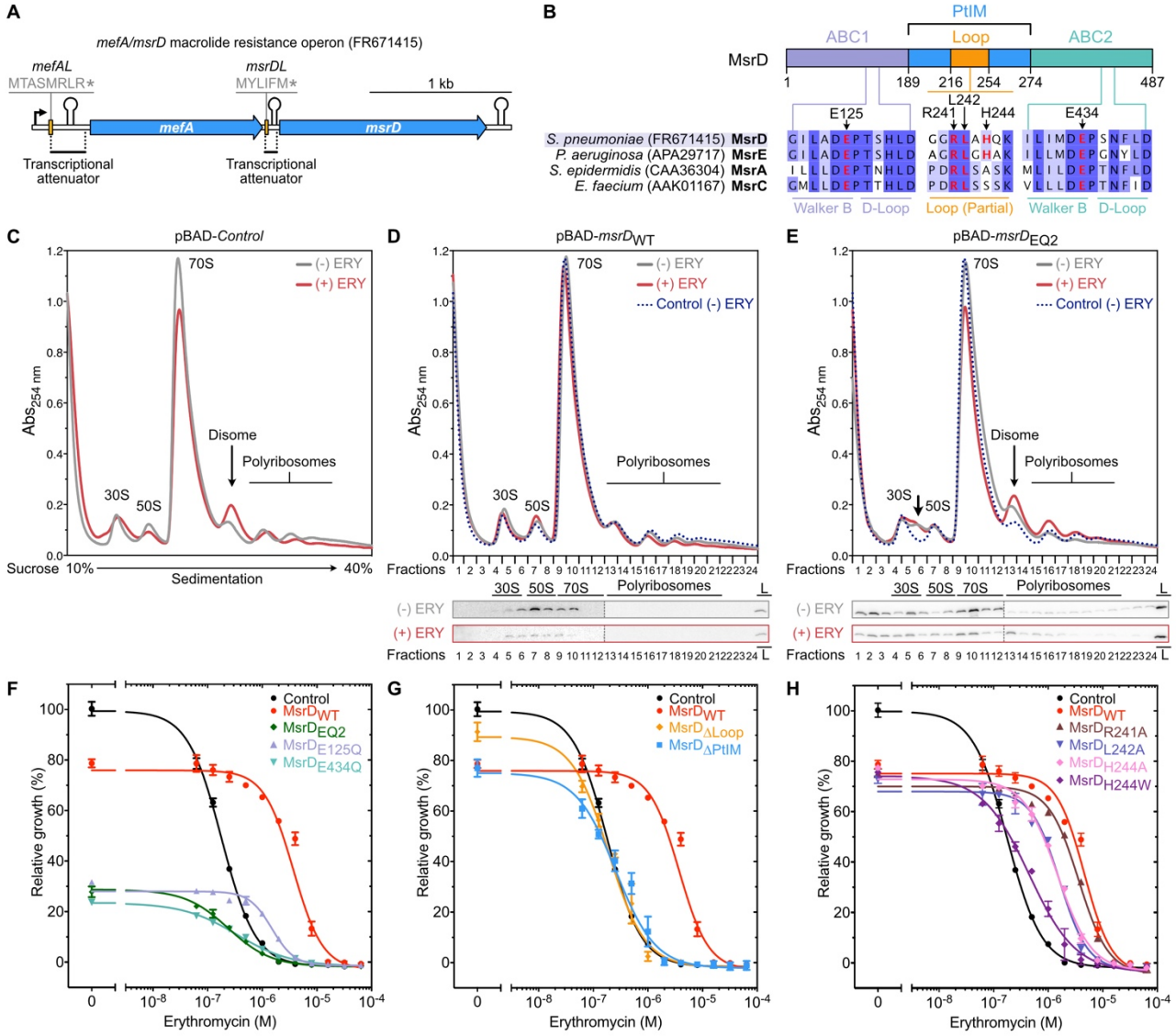

1190

FIGURE 2

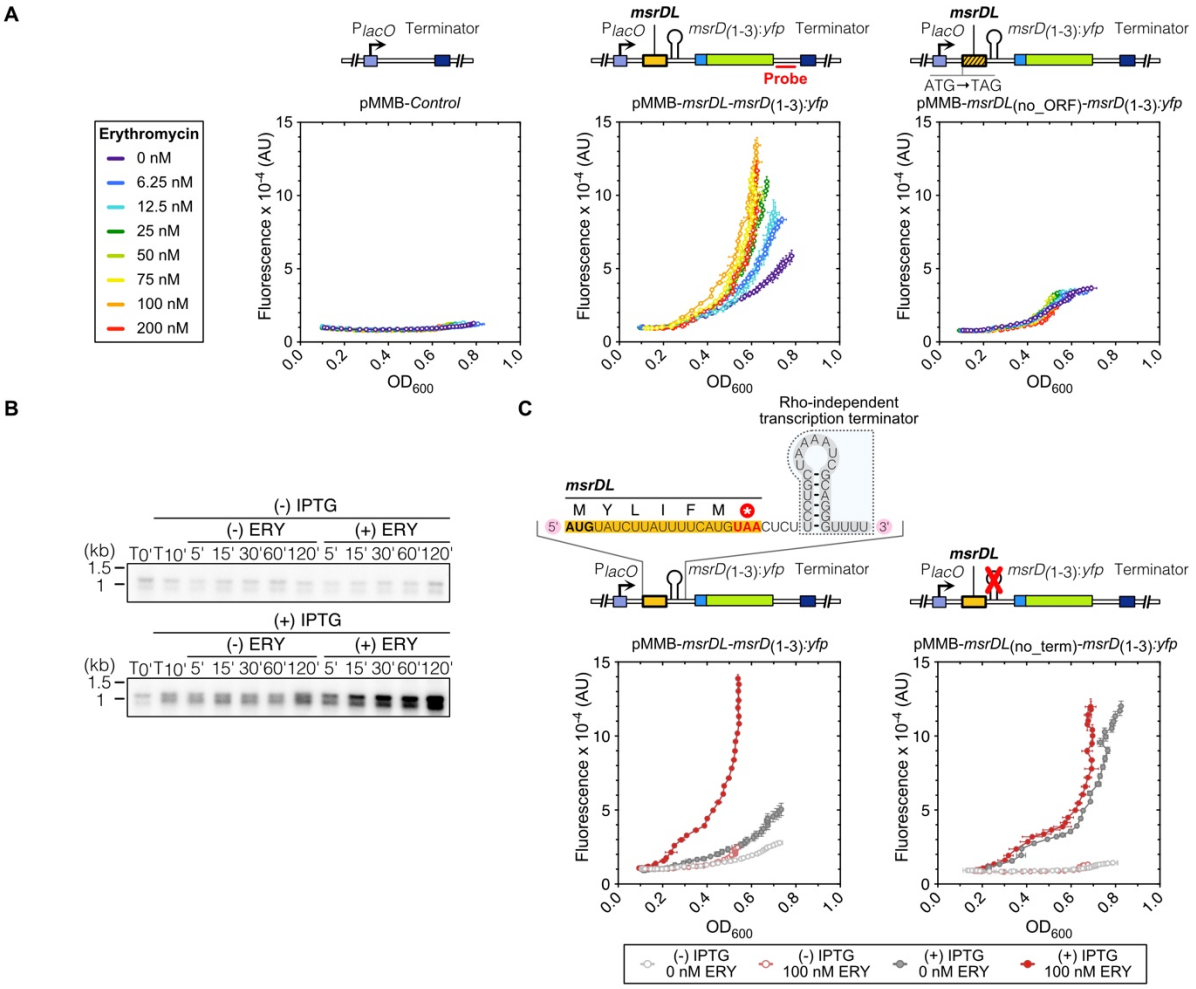

1191

FIGURE 3

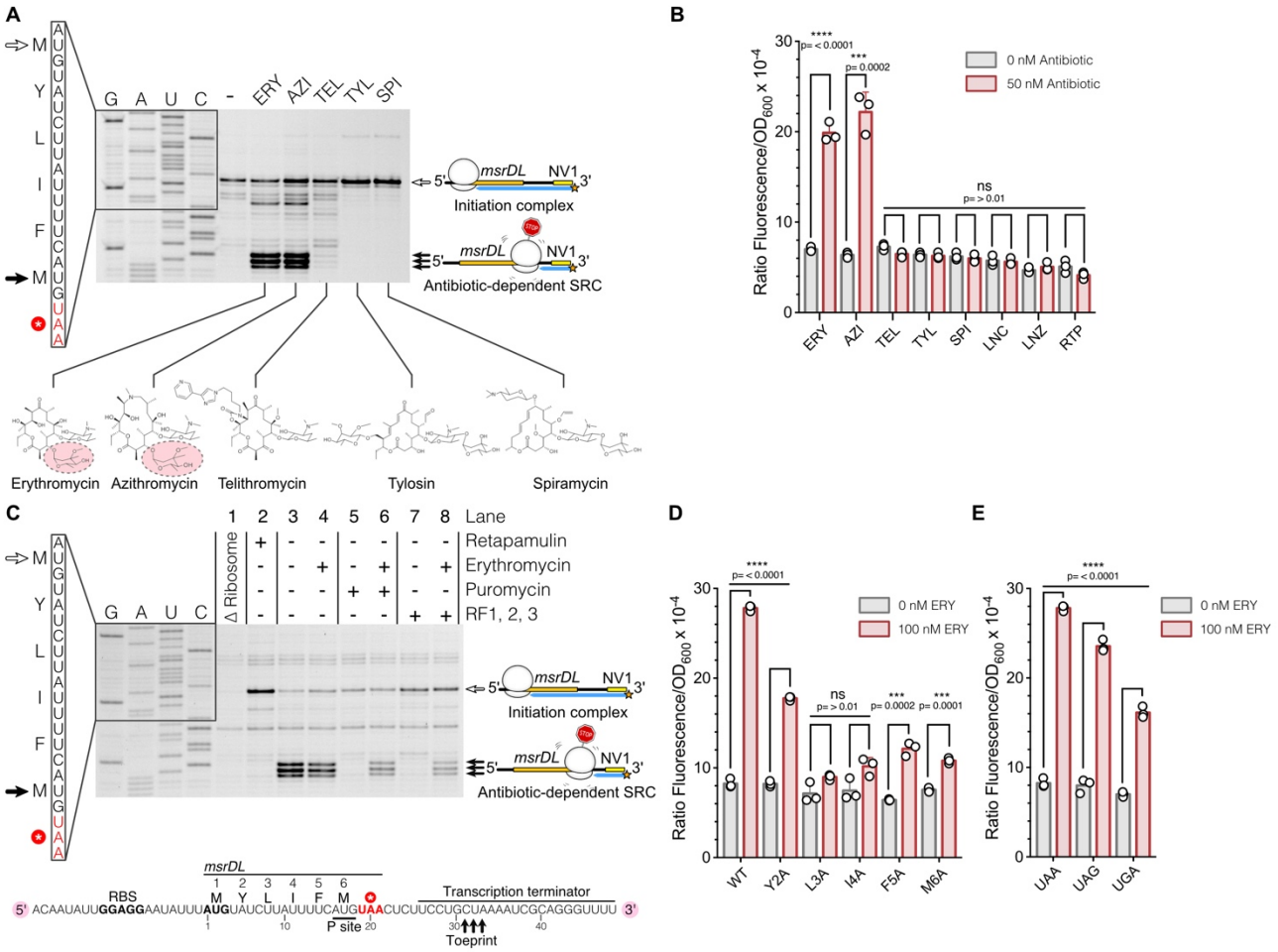

1192

FIGURE 4

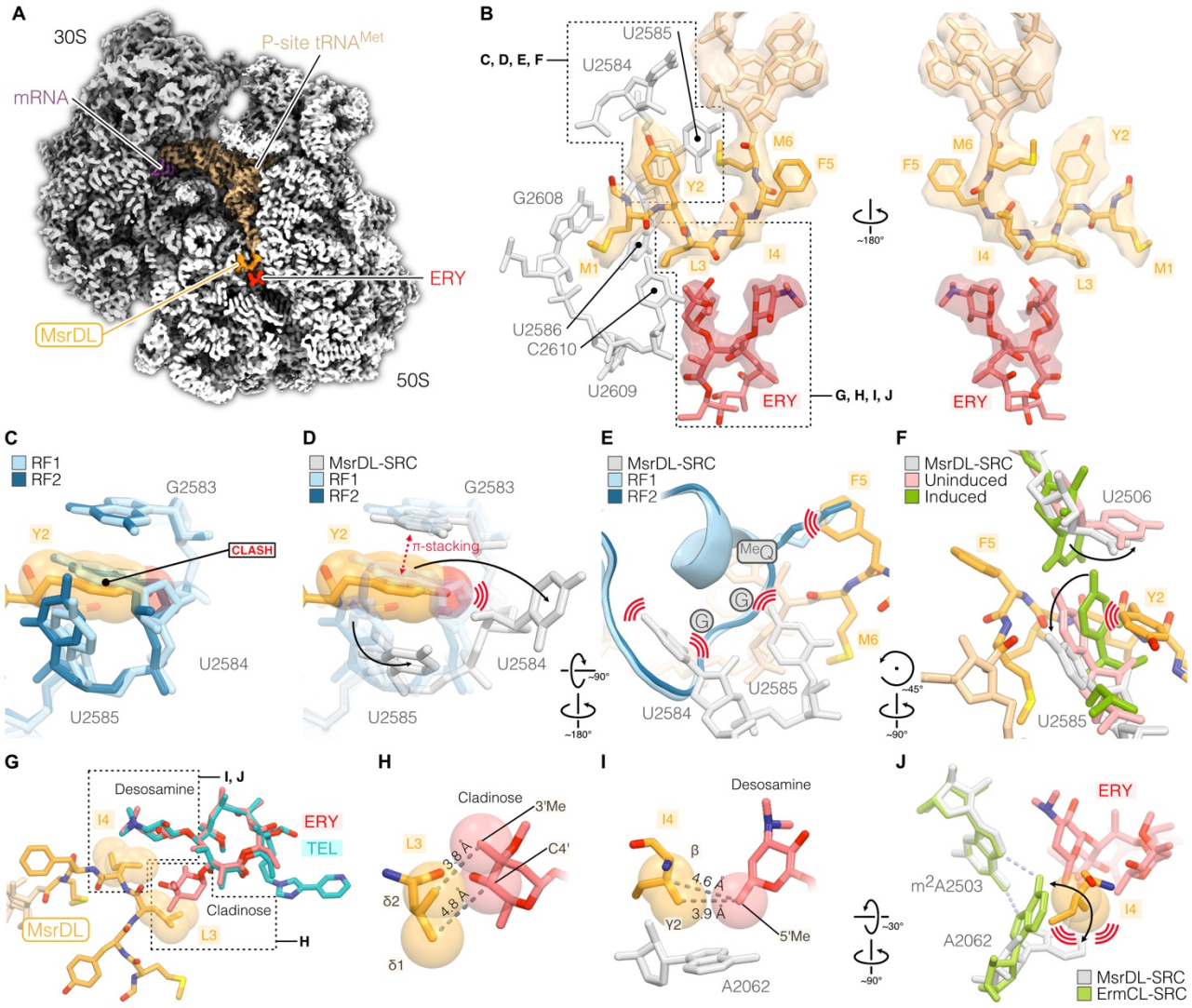

1193

FIGURE 5

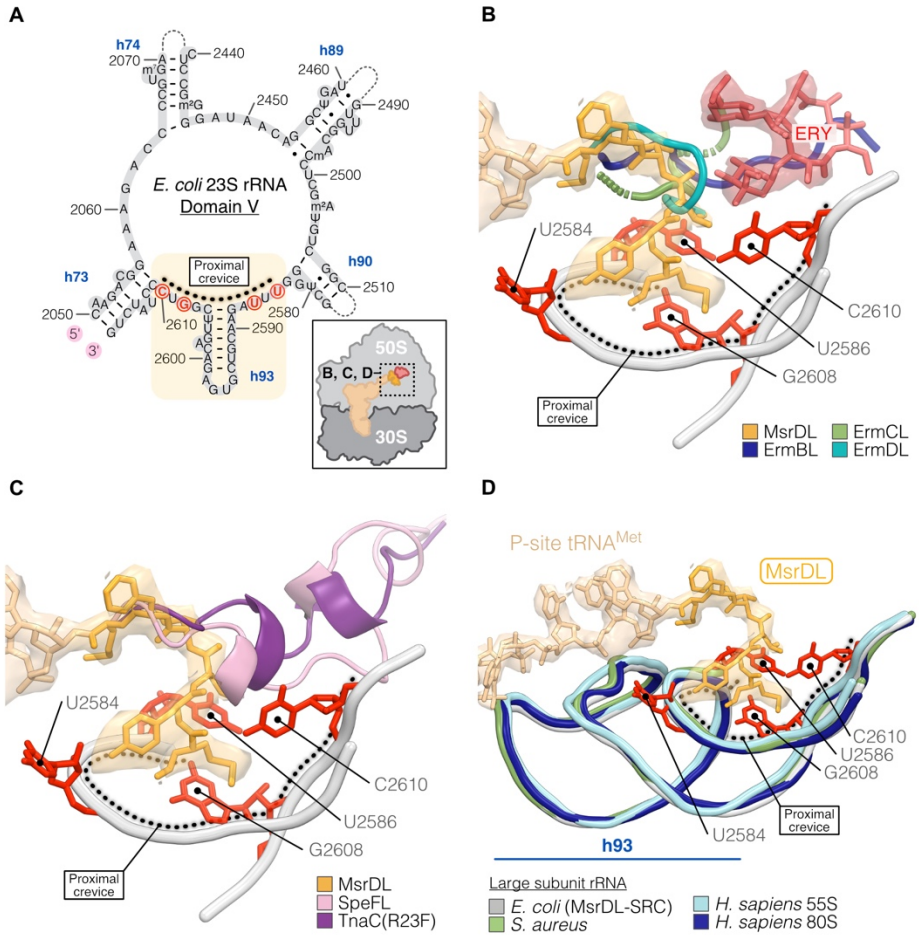

1194
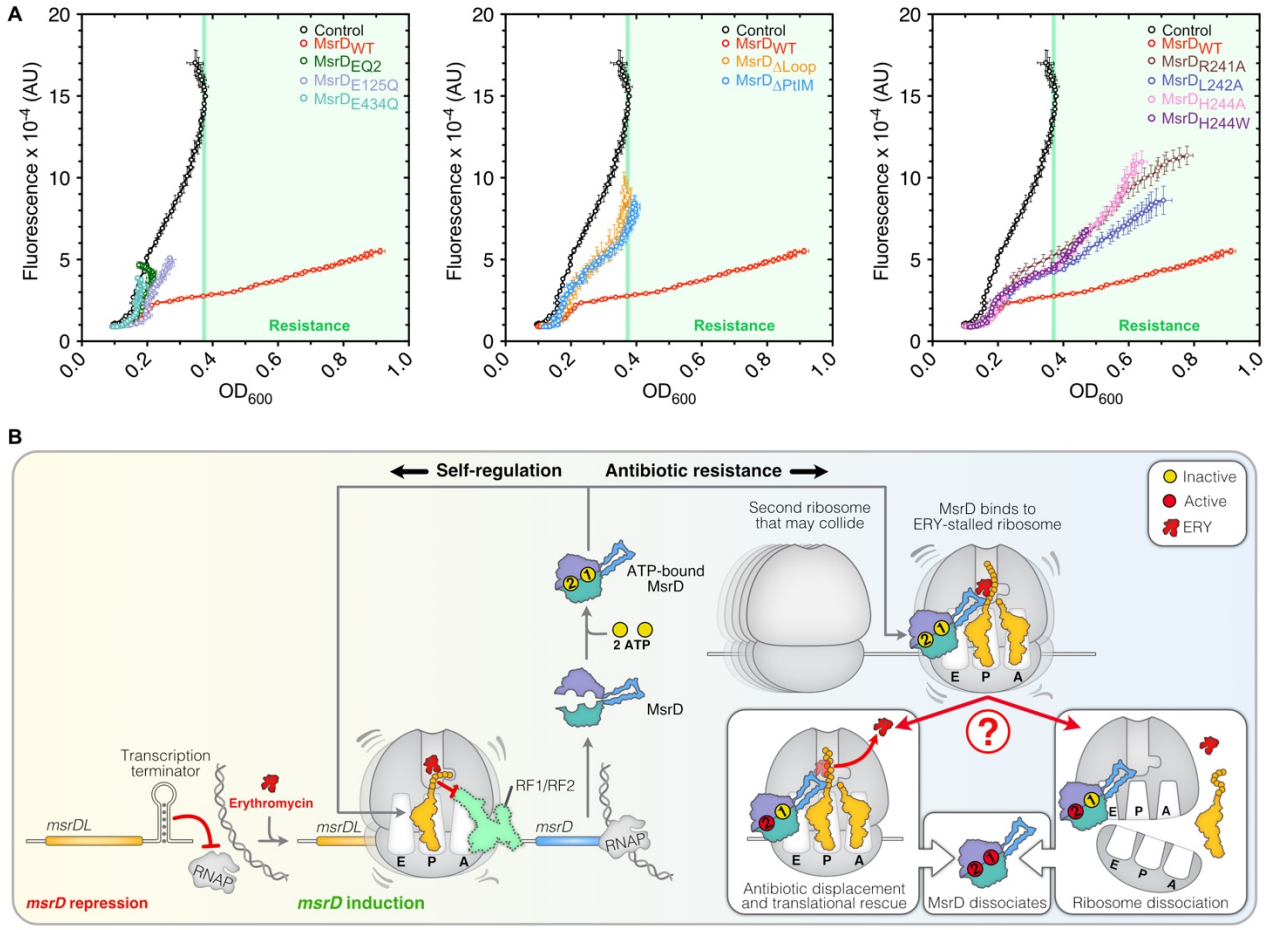
FIGURE 6